FACULTY OF SCIENCE
UNIVERSITY OF COPENHAGEN

Thesis for the degree Candidatus Scientiarum in Physics

Magnus E. L. Kristensen

NEGIS Phosphate and pH measurements

First continuous Phosphate and pH record from a Greenland shallow ice core

Supervisors:
Anders Svensson, Paul T. Vallelona and Helle A. Kjær
Centre for Ice and Climate, Niels Bohr Institute
University of Copenhagen, Denmark

Submitted: 04/09/13

Master's Thesis

Title:	First Continuous Phosphate and pH records from a Greenland shallow ice core
ECTS-points:	30
Superviser:	Anders Svensson Helle Astrid Kjær Paul Travis Vallelonga
Name of department:	Centre for Ice and Climate Niels Bohr Institute University of Copenhagen
Signature:	_____
Author:	Magnus E.L. Kristensen
Submitted:	4th of September, 2013

Abstract

Ice cores has long been used as a reliable and precise archive of past climate conditions, and the analysis of them provide information on a range of processes from global air temperatures and the atmospheric composition to the extent of wildfires in North America and biological activity levels in the oceans. In the present study new techniques was applied to a shallow ice core in order to measure the phosphate content and the pH level of the ice. Neither of these measurements are standard procedures for the continuous flow analysis (CFA) setup, and the present study is the first continuous phosphate and pH record from a Greenland ice core.

Phosphate is an important and possibly limiting nutrient for primary production in the oceans. Because of human activities such as widespread use of fertilizers and conversion of forest and grasslands into farmland, many changes to the phosphate cycle has occurred over the last centuries, the extent of which is not known exactly. Analysing phosphate concentrations in ice cores may help gain important knowledge about the extent of those processes.

pH on the other hand is a master variable that strongly influences as varied processes as the solubility and hence the weathering of minerals, the speciation of aerosols and the equilibrium concentration of any chemical reaction that involves the hydrogen ion. The pH is however usually estimated from the conductivity of ice and melt water rather than measuring the actual pH. It is however believed that there is a strong relation between these measures, and conductivity measurements has the advantage of being both faster than pH measurements as well as being non destructive.

A continuous and highly sensitive absorption method developed by Kjær [2010] (for phosphate) and Raghuraman et al. [2006] (for pH) was applied to the detection of both of these species in ice cores. The ice core analysed was the NEGIS shallow ice core from the Greenland ice sheet, which covers the past 400 years. Results showed that the average level of phosphate in the NEGIS core was 0.32 ppb, and no clear indications of anthropogenic changes was found. A high correlation between phosphate and dust as well as between phosphate and pH suggests that dust is either a source or a transport mechanism for phosphate, and that the acidity level may alter the solubility of atmospheric dust to release more phosphorus.

The relation between the pH measurements and the electrical conductivity measurements was investigated, and all previously observed trends from the literature regarding these relations was confirmed. The relation, though, has been developed for use with ice cores, and the application on the much less dense firn core requires some alterations to the relation.

Dansk Resumé

I iskerner er nedbør fra tidligere tider blevet gemt i årlag. Ved at måle indholdet af forskellige kemiske urenheder i isen og andre fysiske karakteristika, er det muligt at blive klogere for fortidens klima og atmosfæriske forhold, og iskerner har derfor længe været brugt som et arkiv over tidligere tiders klima. Mange typer af kemisk urenheder er blevet målt, men i nærværende tese er nye metoder blevet anvendt til at måle indholdet af fosfat samt til at afmåle pH af isen.

Fosfat er et vigtigt næringsstof for liv, og til tider kan det endog være en begrænsende faktor for vækst i biologiske systemer, specielt vigtigt er det for primærproduktionen i havene. På grund skovrydning og brug af fosfat som gødskningsstof, har man i de sidste århundrede kunnet se store forandringer i fosforkredsløbet, og målinger af fosfat koncentrationen i iskerner kan muligvis hjælpe med at bedømme hvor stor en effekt menneskeskabte påvirkninger har haft, samt indikerer niveauet af biologiske aktivitet i havene. Da det hverken er standard at måle fosfat eller pH direkte på iskerner, er der ikke mange studier der har beskæftiget sig med dette emne, og nærværende afhandling er da også den første af sin slags, med kontinuerte målinger for en hel kort iskerne. Dog er der tidligere blevet målt fosfat på brudstykker af iskerner, hvorfra der er fundet middelkoncentrationer på mellem 0.25 ppb og 0.32 ppb, [Edwards et al., 2007; Kjær, 2010]. pH niveauet er mere variabelt, og bruges generelt som indikation på øget bioaktivitet og vulkanske udbrud.

Den atmosfæriske pH har en stor betydning for opløseligheden af mange mineraler samt atmosfærisk kemi og ligevægtskoncentrationer, og har derfor stor betydning for hvordan data fra iskerner skal fortolkes. Dog er det standard at foretage pH målinger indirekte, ved at måle den elektriske konduktivitet af isen, snarere end indholdet af hydrogen ioner. Dog er der en klar relation mellem disse størrelser, og konduktivitetsmålingerne har desuden den fordel at de ikke er destruktive. Det er dog ikke altid at de to mål stemmer helt overens, og nogle af disse forskelle behandles i denne rapport.

Kontinuerte og meget følsomme absorptions målemetoder blev benyttet til måling af både fosfat og pH. Metoderne er udviklet af respektivt Kjær [2010] og Raghuraman et al. [2006]. Den analyserede iskerne var den korte NEGIS iskerne fra den Grønlandske iskappe, og kernen dækker over de sidste 400 års klimahistorie. Resultatet af målingerne viser at den gennemsnitlige koncentration af fosfat i denne iskerne var 0.32 ppb, og at det endvidere ikke var muligt at se nogen menneskeskabte effekter inden for usikkerheden af målingerne. Det viste sig at der var en stærk korrelation mellem både mængden af fosfat og mængden af støv, samt mellem fosfat og prøvens pH værdi. Dette tyder på at støv er enten en kilde til fosfat i iskerner, eller at fosfat bliver transporteret til iskappen af samme vej som støvet. Korrelationen til pH indikerer desuden at opløseligheden af fosfat fra eksempelvist støv kan ændre sig med pH.

Der er tidligere lavet mange studier af hvordan pH og konduktivitet af en iskerne er relateret, og alle tidligere observerede tendenser kunne genfindes i målingerne for NEGIS ker-

nen. Mange af de relationer mellem pH og konduktivitet der tidligere er blevet foreslået, er dog blevet foreslået på baggrund af egentlige iskernemålinger. Da NEGIS er en kort kerne, er densiteten af firnen meget lavere end for is, og det har derfor været nødvendigt at foretage korrektioner baseret på denne forskel.

Preface and Acknowledgement

This thesis represents the final assignment concluding the Author's Masters Degree in Physics at the University of Copenhagen. The project was carried out at the Centre for Ice and Climate under the supervision of Anders Svensson, Paul T. Vallelonga and Helle A. Kjær. It is a 30 ETCS project and had the time frame of half a year.

I am very grateful for all the help and encouragement I have received in all stages of this project. I would like to acknowledge my supervisors for providing inspiring and motivating supervision during all stages of this thesis, and for always having an open door. I also owe many thanks to the other members of the CFA laboratory: Paul Vallelonga, Helle Kjær, Tibuleac Catalin, Trevor Popp and Rebecca Smith, for a good working environment and for advice on the experimental part of the project, and to Anders Svensson and Tibuleac Catalin for conducting the density measurements and the ECM and DEP measurements. In addition, I would like to thank Lisbeth T. Nielsen for helpful comments and proofreading of the final report.

Magnus E. L. Kristensen
University of Copenhagen, September 2013

Contents

CHAPTER

1 Introduction

In the summer of 2012 a 70 metre shallow firn/ice core was drilled on the Greenland ice sheet at the site 75.623°N, 35.96°W, [Larsen et al., 2012], situated on the North Eastern Greenland Ice Stream (NEGIS), the biggest ice stream in Greenland, in order to investigate the flow patterns of the stream and to test new analytical techniques. Also, van den Broeke et al. [2009] has estimated that approximately 50 % of the Greenland ice sheet mass loss is due to ice stream discharges, which makes it important to understand the stability of the ice streams in order to make reliable predictions about the future mass loss and the ensuing rise in sea level. A map of the location of the NEGIS site is shown in figure 1. During the autumn of 2012 the core was processed at the Niels Bohr Institute (NBI), where density and electrical conductivity profiles were obtained, and in the spring of 2013 the samples were processed with a continuous flow analysis (CFA) setup for the content of water isotopes, chemical impurities and dust using existing analytical equipment at the Centre for Ice and Climate (CIC).

Recently, new analytical techniques for continuous analysis of phosphate and acidity in ice cores has been developed at CIC [Kjær, 2010]. However, phosphate has a very low concentration in the ice, and is thus very challenging to measure accurately, and the new NEGIS record will be the first of its kind with phosphate measurements spanning the whole shallow core. Based on this phosphate record, this thesis aims to determine the average central Greenland phosphate deposition flux over the last centuries, to examine the seasonality of the phosphate deposition and the association of phosphate with other ice core impurities, as well as to investigate whether there has been any anthropogenic influence on the phosphate concentration in the Greenland ice sheet.

In the case of acidity measurements, several methods is available for continuous measurements of ice cores. However, the NEGIS record is the first to use a colorimetric approach. This acidity record has been used to explore CO_2 calibration issues, and to compare these measurements to NEGIS Electrical Conductivity Measurements (ECM), DiElectric Profiling (DEP) methods as well as to the electrolytic melt water conductivity, in order to investigate

the differences between these conductivity measurements.

For this thesis, measurements and data analysis of phosphate and acidity was conducted, while measurements for other chemical constituents was carried out by other members of the CFA laboratory.

Phosphate is a very important element in the biosphere, believed to be a limiting factor of primary production, while acidity is an indicator of biogenic, as well as volcanic, activity. In **Chapter** 2 a short introduction to the relevance of measuring phosphate and acidity in ice cores in an effort to constrain the biogenic activity of the past is presented. Also a short overview of the phosphorus cycle is given. **Chapter** 3 seeks to explain why ice cores can be used as climate archives of the past, and what information can be gained by studying them. **Chapter** 4 provides information on the experimental techniques used in this project for the detection of ions in ice cores, specifically the method of continuous flow analysis. This section also includes information on the specific CFA setup that was used for this thesis. In **Chapter** 5 information on the NEGIS site can be found, along with a description of how the measurements were conducted. In **Chapter** 6 the data and results obtained from measurements of the shallow firn/ice core from the NEGIS site is presented and discussed. In **Chapter** 7 the findings are summarized, and suggestions for further studies are made.

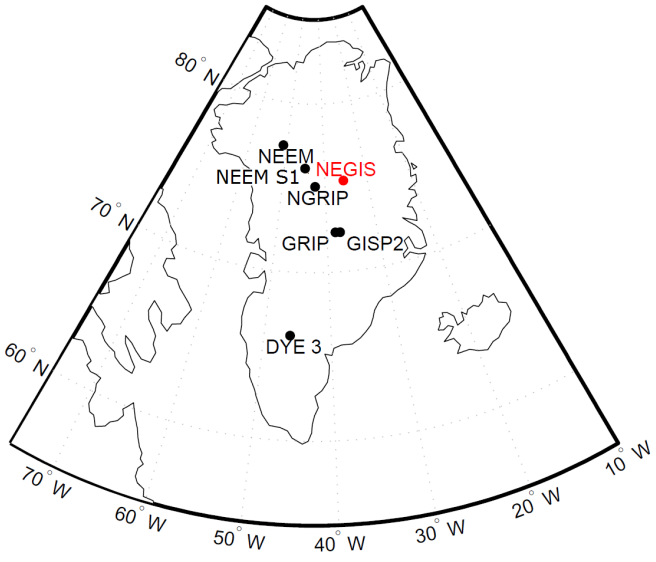

Figure 1: Location of the NEGIS shallow core drill site in relation to some of the earlier drill sites. The figure is from Kjær et al. [2012a].

CHAPTER

2 Background

In this section, background information on the chemical species of interest to this project is given as a motivation for the following chapters. As we will see in **Chapter** 3, ice cores can be used as an archive of past climatic conditions, based on measurements of the chemical impurities that are present in the ice. Measurements of many of these impurities have been made standard procedures in ice core analysis, but new techniques can produce more accurate data, and detection of new chemical species may provide new information altogether.

2.1 Phosphorus

Although phosphorus (P) is a relatively rare element in the Earth's crust (0.09 wt%, [Filippelli, 2008; Paytan and McLaughlin, 2007]) and in the biosphere, it has many important roles in the chemistry of life, and is a part of all living organisms, [Filippelli, 2002]. It is an integral part of bone matter and teeth, it is present in the phospholipids that make up cell wall membranes, a number of enzymes, hormones and cell signalling molecules depend on phosphorylation for their activation, it is an important part of nucleic acids (DNA and RNA) and of adenosine triphosphate, the life's carrier of energy, [Estela and Cerdá, 2005; Filippelli, 2008; Paytan and McLaughlin, 2007; Smil, 2002]. Moreover, Earth's biological systems have depended on P since the beginning of life [Filippelli, 2008]. The majority of the phosphorus in living organisms are found as phosphate, PO_4, [Estela and Cerdá, 2005; Paytan and McLaughlin, 2007].

Unlike the other building blocks of life – carbon, nitrogen and sulphur – phosphorus does not form any long lived atmospheric compounds on which its transport can depend, [Mahowald et al., 2008]. It is only released slowly from minerals during weathering, [Filippelli, 2008; Paytan and McLaughlin, 2007], and even then it is quickly sequestered into a number of less accessible phases, limiting its day-to-day availability to plants and organisms, [Filippelli, 2002]. Hence on a large scale, its global cycle simply follows the slow processes of denudation and geotectonic uplift, [Smil, 2002]. On a smaller scale though, phosphorus is

rapidly and extensively recycled between organic and inorganic forms in soils and in water bodies, [Filippelli, 2008; Smil, 2002]. Since phosphorus does not have a stable gaseous phase, its aerial transport is reduced to transportation by aerosols such as dust, [Filippelli, 2008; Mahowald et al., 2008].

It appears that phosphorus is a very important element with respect to the growth of the biosphere, and hence by measuring past P fluxes, it might be possible to put constraints on past biogenic activity levels. To do this, one will need to know both how P is cycled and transported on Earth, and how it is transported and deposited in our climatic archive in the ice sheets.

2.1.1 The phosphorus cylce

In this section a short overview of the phosphorus cycle can be found, in order to describe the different transport mechanisms that can take the phosphorus to the interior of the Greenland ice sheet. From the literature it is found that sea salt, dust particles and possibly ash from forest fires, [Mahowald et al., 2008; Nenes et al., 2011; Smil, 2002] as well as the occasional volcanic eruption, [Cole-Dai, 2010; Paytan and McLaughlin, 2007], may be sources of phosphorus in ice cores. A schematic overview of the cycle and interactions can be found in figure 3 on page 11, and from this it is clear that the sources and transportation patterns are numerous and varied. Typical concentrations of P is 700 – 1300 mg/kg in the Earth's crust as well as in dust, depending on the source area. Saharan dust has been measured at 720 ppm, Spanish soils at 940 ppm and the fertilized fields of Asia at 1090 ppm, [Mahowald et al., 2008]. Ocean surface waters contain 0.05 - 3.5 μM P (1.6 to 108 ppb) and there is 0.12 to 378 ng/m^3 in the atmosphere, [Mahowald et al., 2008]. Here M is mol/L, which can be converted to ppb (parts per billion) (ng/g) by using the molar weight of phosphorus and phosphate respectively.

The P fluxes and the total amount of phosphorus in any given part of the global phosphorus cycle can be found in [Paytan and McLaughlin, 2007; Smil, 2002], which also includes estimates of the anthropogenic contributions. A table containing the most important numbers, as found by Smil [2002], can be found in table 1, although numbers do seem to vary between papers with different numbers being reported by Paytan and McLaughlin [2007] and Bolin et al. [1981].

Phosphorus on land

As mentioned above, phosphorus is only present in very small amounts in the Earth's crust, being the eleventh most abundant element, [Filippelli, 2002], and is only present in appreciable amounts in a few minerals, with apatite [$Ca_5(PO_4)_{3-}$(F,Cl,OH)] being the most common naturally occurring source in the Earth's crust, holding more than 95 % of the P reserves, [Paytan and McLaughlin, 2007]. Soluble phosphates are released by weathering of apatite minerals, as a result of a reaction with dissolved carbon dioxide in the form of carbonic acid, [Filippelli, 2008]:

Phosphorus reservoirs	**Total storage (Mt P)**
Ocean	93000
Surface	8000
Deep	85000
Soils	40–50
Inorganic phosphorus	35–40
Organic phosphorus	5–10
Phytomass	570–625
Terrestrial	500–550
Marine	70–75
Zoomass	30–50
Anthropomass	3

Phosphorus fluxes	**Annual rate (Mt P year^{-1})**
Atmospheric deposition	3–4
Erosion and runoff	25–30
Particulate phosphorus	18–22
Dissolved phosphorus	2–3
Plant uptake	970–1300
Terrestrial	70–100
Marine	900–1200
Burial in marine sediments	20–35
Tectonic uplift	15–25

Table 1: Overview of the major biosphere reservoirs and fluxes of phosphorus. The table is from [Smil, 2002].

$$Ca_5(PO_4)_3OH + 4H_2CO_3 \rightleftharpoons 5Ca^{2+} + 3HPO_4^{2-} + 4HCO_3^- + H_2O. \tag{2.1}$$

The released phosphorus is then free to be absorbed into the biosphere or transported to other regions as dust or in aqueous solution. In soils weathering can release phosphorus through several processes: biochemical respiratory processes release CO_2 that increases the acidity in the vicinity of the plant roots, and this releases the crystalline P according to equation (2.1). Alternatively plant roots can produce organic acid and/or phosphatase enzymes themselves, [Filippelli, 2002]. Even though soluble phosphates are released by weathering, they are rapidly transformed to insoluble compounds, due to weathering co-precipitation of e.g. iron and manganese oxyhydroxides, that have a large potential for binding phosphate [Filippelli, 2008]. Only the dissolved reactive phosphorus (DRP) can be absorbed by the biosphere, [Paytan and McLaughlin, 2007], and therefore only this fraction of the total phosphorus amount is of interest in this study. Soluble reactive phosphorus is defined as the dissolved P fraction that reacts in an acid solution containing molybdate ions to form a phosphor-molybdate complex, which then forms a coloured molybdenum blue complex when reduced with ascorbic acid, [Paytan and McLaughlin, 2007]. DRP is mostly in the form

of orthophosphate, PO_4^{3-}.

The most significant transfer of PO_4^{3-} is by riverine transport of eroded soil to the oceans, [Paytan and McLaughlin, 2007]. In rivers phosphate occurs in dissolved and particulate forms, [Paytan and McLaughlin, 2007]. In the particulate form P is held in a mineral lattice, and cannot actively take part of the biochemical cycle. This is also true when the mineral reaches the sea, as both pH values and ionic buffering is strong, which makes the dissolution rate very low, Filippelli [2008]. As a result, much of the P that is eroded from the continents reach the ocean in much the same state as it left, and is therefore simply left as sediments on the coastal margins. Only about 10-30 % of the P transported by rivers will end up being available to the marine biosphere, [Paytan and McLaughlin, 2007].

Phosphorus in biological systems

Along with nitrogen, potassium and carbon, phosphorus is one of the critical macro nutrients needed by all living organisms, [Smil, 2002], and can therefore be a limiting element in ecosystems, although how limiting is the subject of some research. Phosphorus may set an upper limit on the amount of organic matter that can be produced, but at any given point in time and space, it may be that another element, such as the amount of nutrients, that limits the system [Paytan and McLaughlin, 2007]. Some plant species are able to fix nitrogen from the atmosphere, and therefore phosphorus would seem to be the only truly limiting element of the major nutrients [Bolin et al., 1981; Nenes et al., 2011], since the biosphere can accommodate any long-term nitrogen deficiency by increasing nitrogen fixation from the atmosphere, [Filippelli, 2002; Nenes et al., 2011; Paytan and McLaughlin, 2007]. This can be made explicit by looking at the average ocean photosynthesis, described by Paytan and McLaughlin [2007], where phosphorus in the form of orthophosphate plays a key role. Under the influence of trace elements, vitamins and light, the chemical equation of photosynthesis is

$$106\,CO_2 + 16\,HNO_3 + H_3PO_4 \rightarrow C_{106}H_{263}O_{110}N_{16}P + 138O_2, \tag{2.2}$$

where the elements carbon, nitrogen and phosphorus appear in the Redfield ratio, 106:16:1. Given the scarcity of biochemically available phosphorus in the ocean, this means that the marine biosphere can strongly influence the marine carbon cycle and the drawdown of atmospheric carbon dioxide [Paytan and McLaughlin, 2007]. The drawdown is facilitated by a process known as the biological pump, in which carbon dioxide is pumped from the euphotic zone in the oceans to the deep oceans in the form of organic carbon, such as dead organism, by the marine life, [Kjær, 2010; Paytan and McLaughlin, 2007]. It has been estimated that phosphorus fluxes could facilitate as much as 264 T moles yearly oceanic uptake of CO_2, [Nenes et al., 2011]. This means that phosphate concentrations can influence the global climate by being the limiting element in the photosynthesis, and hence the biological pump.

Since phosphate is often the limiting nutrient in aquatic productivity, and because a single atom of phosphorus according to the Redfield ratio supports the production of as much phytomass as 106 atoms of carbon and 16 atoms of nitrogen, this means that even in the relatively low concentrations present in the runoff from fertilized fields, it can cause eutrophication (excessive nutritional enrichment), in both fresh water and in ocean water,[Smil, 2002]. Constant mixing and a lack of absorbing surfaces makes P in water bodies much more readily available to living organisms than soil based P, [Kjær, 2010; Smil, 2002].

On a land based scale, phosphorus from biological systems may enter the global circulation that could take it to the ice sheets, as a result of biomass burning such as wildfires, since biogenic material is rich on phosphate, [Mahowald et al., 2008; Nenes et al., 2011; Smil, 2002]. Primary biogenic particles are essentially just spores and plant bits which can also be emitted directly into the atmosphere. According to Mahowald et al. [2008] these biogenic sources can be identified by substantial amounts of potassium, K, as well, and dust, biogenic particles and biomass burning may be distinguished by the size distribution of the K aerosols.

Oceanic phosphorus

In the ocean, the phosphorus input and output is driven to a steady state mass balance by biological productivity, [Filippelli, 2008]. In most surface waters, the phosphate concentration will be near zero, as the element is absorbed into the biosphere by phytoplanktonic activity, although surface concentrations may vary with both location and with the season, [Filippelli, 2008; Mahowald et al., 2008]. According to Filippelli [2002], P concentration also varies with age of deep waters, and thus the relatively young deep water of the Atlantic has concentrations of $\sim 1.5\ \mu$M, whereas the older pacific water has concentrations of $\sim 2.5\ \mu$M. When sedimented on the continental margins and in the deep sees, P will remain inaccessible to the biosphere until subduction or accretion eventually returns it to be exposed on land again, on a timescale of $10^6 - 10^7$ years, [Smil, 2002].

From the ocean, phosphorus may be brought to the ice sheets, along with sea salt from sea sprays, with water droplets working as aerosols [Kjær et al., 2011; Mahowald et al., 2008]. As a result of increased wind speeds during winter time, the sodium record will show distinct seasonal variations, [Kjær et al., 2011].

Generally sea salt aerosols have a broad range of phosphate concentrations, but the contribution from sea salt aerosols to the total P flux may be calculated by assuming that sea salt has the same range of P concentration values as surface waters does, which as mentioned has been estimated at 1.6 to 108 ppb, [Mahowald et al., 2008].

Atmospheric phosphorus

Since P does not have a gaseous phase, most of the atmospheric phosphorus is associated with mineral aerosols, i.e. dust particles derived from soil erosion of cleared land, [Mahowald et al., 2008; Nenes et al., 2011].

Not all of the phosphorus transported by aerosols may be available for primary production, as both source area, deposition type and solubility in water with different pH and salt levels may influence the availability at the deposition site, [Mahowald et al., 2008; Nenes et al., 2011]. As mentioned above, Mahowald et al. [2008] has estimated the average concentration of P in the Earths crust to be 700 ppm with values up to about 1300 ppm depending on source area. According to Paytan and McLaughlin [2007] the amount of P in dust is similar to the crustal abundance, and finally Mahowald et al. [2008] has found that the soluble fraction of the total phosphate in dust may range between 7-100%. On a global scale the sources for phosphorus have been estimated by Mahowald et al. [2008] to be 82 % mineral aerosols, 12 % are biogenic particles and a further 5 % comes from combustion sources.

Volcanoes may also contribute to the total phosphorus flux, [Mahowald et al., 2008; Nenes et al., 2011; Paytan and McLaughlin, 2007], and measurements have shown that volcanic ash contains concentrations of up to 1% P, more than 50 times the background level [Paytan and McLaughlin, 2007], and even have very large flux rates, but eruptions are very localised in scale, so the total contribution to P levels on a global scale is relatively small, [Cole-Dai, 2010; Mahowald et al., 2008].

	Total P (Tg P a^{-1})	PO_4^{3-} (Tg P a^{-1})
Dust	1.150	0.115
Primary biogenic particles	0.164	0.082
Biomass burning	0.025	0.012
Fossil fuels	0.024	0.012
Biofuels	0.021	0.010
Volcanoes	0.006	0.003
Sea salt	0.0049	0.0049
Total	1.39	0.24
Percentage anthropogenic	4.8	14.3

Table 2: Global sources of atmospheric phosphorus. The table is from [Mahowald et al., 2008].

All these aerosols may end up on the ice sheets, but differences in size distributions have a large impact on how and where the deposition takes place, [Mahowald et al., 2008].

Anthropogenic sources

Because anthropogenic influence on the phosphorus cycle began well before any efforts were made to scientifically quantify the P cycle, we can only speculate at the pre-anthropogenic P mass balance, [Filippelli, 2002]. However, Mahowald et al. [2008] has estimated that atmospheric sources of P has changed somewhat as a result of combustion, primary biogenic particles and biomass burning aerosols as new and possibly significant sources of atmospheric phosphorus, and that the global PO_4 transport by rivers has doubled, mostly due to excessive use of fertilizers, as compared to the pre-anthropogenic level. That using fertilizers is an indispensable tool in today's agriculture is exemplified by looking at the quantities consumed.

According to Smil [2002], global food harvest assimilates about 12 Mt P in crops annually, while weathering of rocks and atmospheric deposition supplies only 4 Mt P to the fields. The evolution in global consumption of P in the last century can be found in figure 2.

The anthropogenic phosphate flux has also been increased by the burning of forest and grasslands, where PO_4^{3-} in the form of ash is dissolved and transported by rivers or aerosols [Mahowald et al., 2008; Smil, 2002]. The conversion of forest and grassland into farmland also removes the canopies and litter layers that protects the soil, as the lack of roots destabilizes the PO_4^{3-} rich soils below, with increased soil erosion to follow Smil [2002].

The final major man made contribution to the increase in P levels can be found in combustive processes, where phosphorus may be released when burning bio fuels, [Mahowald et al., 2008]. Even though the trace amounts of phosphorus present in wood and coal remains almost completely in the ash [Smil, 2002], the aerosols have a size much smaller than the aerosols from natural soils. A smaller size facilitates transport over larger distances and with more diffusion meanwhile, [Mahowald et al., 2008].

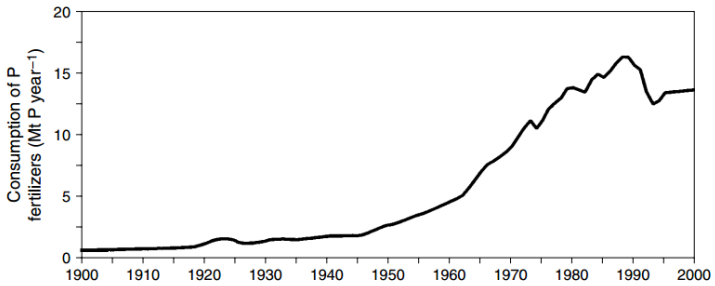

Figure 2: Global consumption of inorganic phosphatic fertilizers, 1900–2000. The figure is from [Smil, 2002].

2.2 pH and the ion balance

The pH in natural systems is a master variable that dictates the solubility of many minerals as well as the equilibrium concentrations of any reaction involving the hydrogen ion. pH is therefore an important indicator of chemical processes occurring in different environments, [Pasteris et al., 2009], and ice cores may provide information on past atmospheric pH conditions. However, using pH measurements as a proxy in ice cores may turn out to be quite difficult, due to samples being under saturated with respect to carbon dioxide, CO_2, immediately after melting, [Pasteris et al., 2012]. This makes it difficult to maintain stable concentrations of dissolved carbon dioxide and hence carbonic acid, H_2CO_3, in the melt water, but any change in the concentration of carbonic acid will impact the pH measurement, [Atkins

and Jones, 2010]. However, when measuring the pH of the ice, it is mostly to be used for constraining on the major ion balance, which CO_2 does not contribute to, and hence the effect of CO_2, on pH at least, should be removed from the data altogether, [Pasteris et al., 2012]. To avoid some of the difficulties, all measurements of pH should be converted into acidity, which is defined as:

$$\text{acidity} = \left[H^+\right] - \left[HCO_3^-\right] - 2\left[CO_3^{2-}\right] - [OH^-], \tag{2.3}$$

as stated in [Pasteris et al., 2012, Supporting Information]. Acidity represents the amount of acid present in a sample besides that which comes from dissolved carbon dioxide, and it is unaffected by changes in activity, CO_2 concentration, temperature and pressure, [Pasteris et al., 2012]. The steps of calculating the acidity can be found in [Atkins and Jones, 2010; National Institute of Standards and Technology, 2013; Pasteris et al., 2012], and is also addressed in **Chapter** 5 of this thesis.

Having converted pH to acidity, ice core acidity turns out to be a proxy for precipitation acidity, [Pasteris et al., 2009], which is an important environmental parameter which as mentioned dictates the solubility of many minerals, and therefore directly affects land surface chemical weathering, soil chemistry, and ecosystem health, [Atkins and Jones, 2010]. It is also a proxy of atmospheric aerosol and gas phase chemistry, in the sense that acidity affects atmospheric processes such as aerosol speciation and the uptake of acids and bases by aerosol particles, [Pasteris et al., 2009]. When coupled to other proxies, the acid content of ice core samples may also provide information on the origin of these acidity levels, including the history of volcanic activity, the biogenic activity levels, windblown dust, forest fires and pollution induced acid rain, [Hammer, 1980; Nenes et al., 2011; Pasteris et al., 2009; Paterson and Cuffey, 2010]. To some extend acidity levels also governs the partitioning of many impurities found in ice cores, and hence detection of pH is essential to fully understand ice core chemistry, [Kjær et al., 2012b].

Many different methods, direct and indirect, of measuring pH has been proposed in the literature, [Pasteris et al., 2012], such as Gran titration, electrical conductivity measurements (ECM), DiElectric Profiling methods (DEP), potentiometric and colorimetric methods. All of these has different advantages and disadvantages, but common to any method to be used to measure pH in ice, is that it requires a high sensitivity, since the range of pH values is narrow, [Pasteris et al., 2012]. Preferably the temporal resolution should be very good as well. In this thesis, a spectrophotometric method was used, see section 5.1.1, due to the flexibility that using different dyes can give, and the result are compared to ECM, DEP and electrolytic melt water conductivity measurements made on the same core in order to quantify their differences.

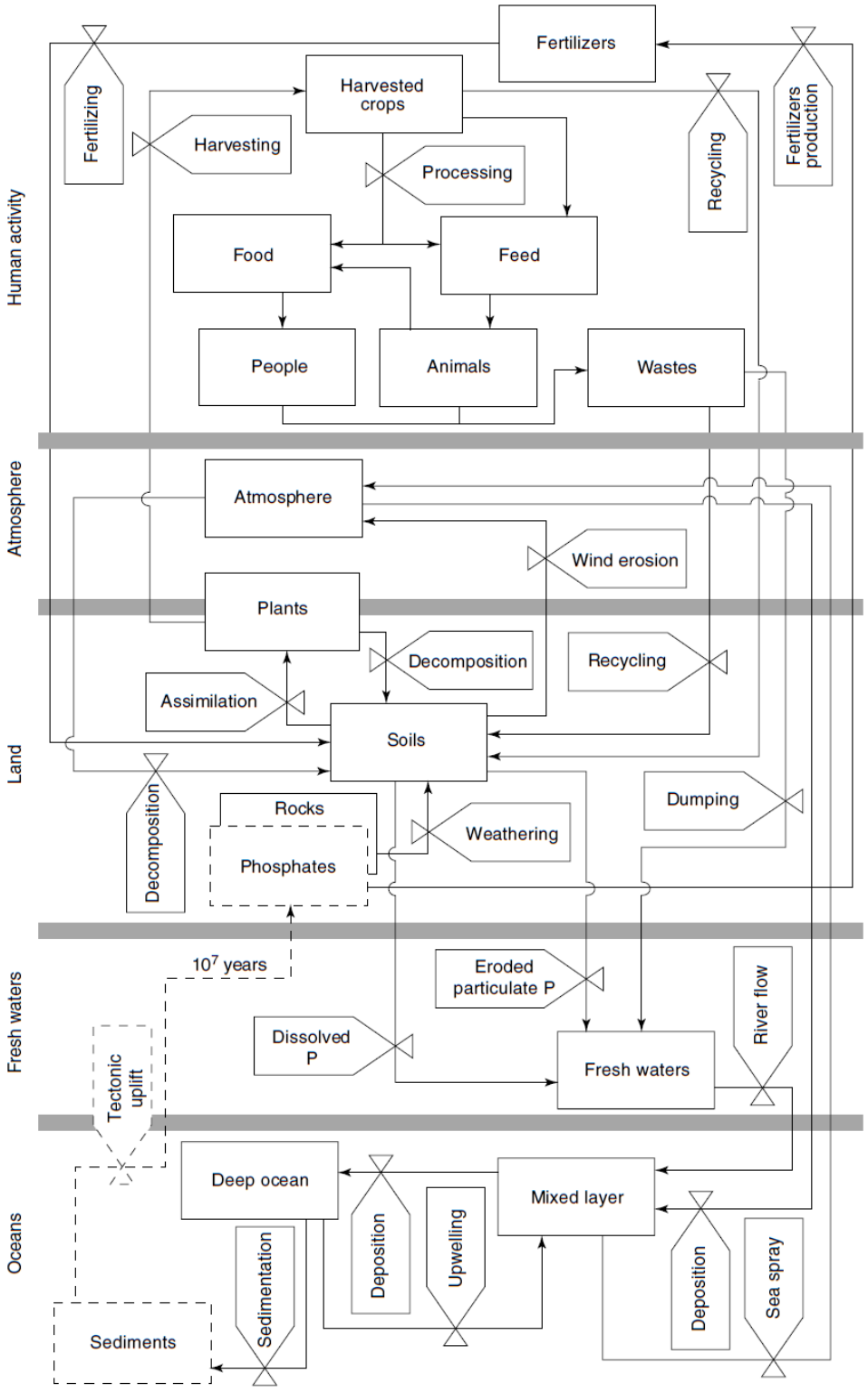

Figure 3: A schematic overview of the global phosphorus cycle. The figure is from Smil [2002].

CHAPTER

3 Ice Cores – A Climate Archive

In this section the question of how and why ice cores can be used as climate archives will be addressed, including the subjects of layering, transportation and deposition processes, how to date the ice cores, and what the different impurities in ice core samples can tell us about the past climate. The leading authority used as a reference for most of this chapter, is Paterson and Cuffey [2010]. Other source texts will be quoted as well when used.

3.1 Layers of the ice sheet

Each year precipitation falls on glaciers and ice sheets, and since melting only occurs when temperatures are above 0°C, snow accumulates and creates a record (of accumulation rates, chemical impurities, temperatures and more) showing how environmental conditions was at the time of precipitation. As new snow falls the following year, layers of ice representing each year will be formed, and hence records from the interior regions of polar ice sheets can provide a very rich view of past climatic conditions in high temporal resolution – depending on the precipitation rate. As the snow slowly densifies to become ice, the air in the snow will eventually be cut off from the atmosphere, and provide a sample of the atmospheric composition at the time of the closure, although some elements such as water vapour are not preserved. Numerous ice core drilling projects in both Greenland and Antarctica has demonstrated the great value of these polar ice sheets as sensitive climate archives of the past atmospheric composition, both for the Holocene and the late Pleistocene, [Bigler et al., 2011]. Greenland ice cores cover the last glacial cycle, [Larsen et al., 2012], whereas Antarctic ice cores archive some 800k years of past climate, [Paterson and Cuffey, 2010]. One should keep in mind though, that many of the properties measured in ice are proxies, and that they vary in response to environmental conditions, but that it does not necessarily preserve the climate signal directly. The interpretation of these proxies may require quite a lot of detective work.

Once the precipitation has been deposited and incorporated in the ice sheet, it is isolated from the present climatic condition, but changes in these conditions may still affect the present composition, as well as transportation and deposition patterns. This means that ice cores may not only provide information on past atmospheric compositions, but also about the atmospheric circulation. Furthermore since the temperature in the ice sheet is always below the freezing point, the record is never corrupted by melt that could otherwise blur the record of impurities and trapped gases. Even though ice cores as a climate archive have many advantages, some complications may also be present.

One of the most important complications is that the ice is viscous, and hence over time it will move and deform according to the forces and stresses that is exerted on it due to the gravitational pull. As snow accumulates on the ice sheets every year, the imbalance of mass between the region of accumulation and the ablation zone builds up shear stress, that will eventually cause the glacier to flow towards the ablation zones, as shown by the flow lines in figure 4. This may represent a challenge when trying to interpret the signal obtained from an ice core, since the geographical origin of the ice will most likely change with the depth in the ice sheet, and atmospheric conditions may be very different across the large ice sheets. One way to avoid this problem is to drill at the ice divide, at exactly the point where the ice flow in different directions cancel out and the horizontal flow therefore is neglectable. At this point all the ice from different depths will originate at approximately the same location on the surface. But even this cannot be more than assumed, since the location of the ice divide may very well have changed over time as well. Not least due to the ice sheet, in Greenland at least, being much larger during the Last Glacial Maximum (LGM), extending all the way to the outer shelf, [Kjær, 2010].

Another common feature of ice sheets is that the flow causes the annual layers to stretch and thin under the pressure of the following precipitation layers and the stresses caused by the ice flow. This result in a decrease of the layer thickness with depth, and therefore the temporal resolution on measurements of ice will decrease with its age.

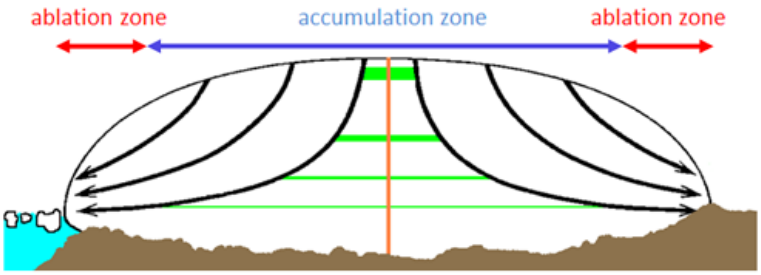

Figure 4: Illustration of how ice will flow from the deposition site and towards the edges of the ice. Annual layers are marked in green, and the ice divide is marked in red. The figure is from [Centre for Ice and Climate, 2013a].

Additional complications, not relevant when analysing a shallow ice core, may be basal melting of the ice, the topography of the bedrock causing changes in flow patterns and, if the bedrock is rough enough, folding of layers with different ages, causing a mixed climate signal in the deepest layers of the ice sheet. Furthermore, some of the physical properties of the ice such as the temperature, the abundance of air bubbles trapped in the ice as well as the thickness of annual layers, are sensitive to the temperature and rate of snowfall at the time and site of precipitation, and these changes in the physical properties of the ice may likewise cause different flow rates of the ice at different depths, complicating the flow further.

3.2 Dating the cores

Dating of the ice cores is an important aspect of analysing the samples, in order to compare information kept in the ice with other climate archives, such as marine cores and dendrochronology, or simply to compare information from different ice cores. The dating of ice cores may in many cases be done in much the same way as counting annual layers in a tree, by recording the seasonal variations of different impurities and properties of the ice, such as δ^{18}O, electrical properties, the concentration of micro particles and dust and variations in the concentration of chemical species, see section 3.4 for an overview of these variables. Using several indicators to create a timeline naturally increases its accuracy.

These layer counting techniques may be very precise, but they only work in places where the annual precipitation rate is high enough to support a temporal resolution of the measurements that can separate the layers. As the layers thin with depth, the resolution deteriorates, raising the need for other dating methods for validation of the layer counting methods. This information may come from ice flow computer models tuned to the local boundary conditions or be constrained by various marker horizons, most notably acid or ash layers created by volcanic eruptions of known age.

In places with very little precipitation, such as Dome C in East Antarctica, [Paterson and Cuffey, 2010], most of the precipitation may come in only a few violent storms, which makes annual layer counting impossible. At such locations, the age scale is constructed almost solely on flow models constrained by the marker horizons, but in the very old, very deep layers, the content of various atmospheric gases with known long lifetimes, such as methane, diatomic oxygen and argon, can be used in combination with the above mentioned methods to increase accuracy. For a shallow core from a site that supports annual layer counting, such as NEGIS, the uncertainty on the timescale is neglectable.

3.3 Transportation and deposition

In order for chemical impurities and other tracers to arrive at the ice sheets, transportation to and deposition at the site is needed. This imposes some limitations on the origin of the impurities, as different impurities and aerosols of different sizes tend to settle at different rates,

[Mahowald et al., 2008]. Atmospheric P is mostly associated with dust, which has a residence time in the atmosphere ranging from hours (if the particle diameter is greater than 10 μm) to several weeks (diameters less than 1 μm), [Mahowald et al., 2005], while the most common element that modifies the atmospheric acidity, sulphate aerosols, has a residence time of a few days in the troposphere, [Cole-Dai, 2010]. All residence times further depends strongly on the type and amount of precipitation present, [Mahowald et al., 2005].

As P correlates to dust it is expected that the transportation of P for a large part is identical to those of dust, although sea salt, biogenic material, anthropogenic activities and possibly tracers of forest fires also correlates somewhat to P. The transportation of dust proceeds according to the wind pattern which, today at least, generally comes from west in the summer time, and south-west in the winter time, [Kjær, 2010]. Even though the transportation of dust would seem to be fairly straightforward, the interpretation will in practice be complicated by a large diversity of factors contributing to the records, such as the geography and strength of sources, atmospheric dynamics, processes of nucleation and scavenging in the atmosphere and post depositional changes. The last of these effects, post depositional changes, is mostly due to diffusion and migration that may occur in the firn.

The transition from aerosol to fall out is called deposition, and generally there are two ways that impurities can be deposited on an ice sheet. Either they travel from the atmosphere to the ice sheet surface attached to the precipitation, i.e. on a snowflake or rain droplet, or they may arrive as independent aerosols. These two ways are known as wet and dry deposition respectively. A simple formula to calculate the net flux of impurities onto the ice, can be found in [Paterson and Cuffey, 2010, section 15.10]. The flux can be calculated from ice core measurements as the product of the concentration of impurities in the ice, C_i and the ice accumulation rate, $\dot{b}$. The simplest plausible model is then simply the sum of wet and dry deposition respectively:

$$\dot{b}C_i = k_d C_a + k_w \dot{b} C_a \tag{3.1}$$

where both types of deposition are assumed to depend on the atmospheric concentration, C_a, of the impurity, and the constants is simply a measure of how effective the deposition processes are.

3.4 Impurities and their interpretation

Here an overview of the different impurities, their origin and their interpretation is given. Many impurities have more than one source though, which may complicate the interpretation. For a thorough understanding of the interpretation of impurities and past research achievements, the reader is referred to Mahowald et al. [2008]; Paterson and Cuffey [2010].

δ^{18}O and δD: The isotopic composition of ocean water is very nearly uniform on a global scale. The three most common stable isotopes of water are $H_2{}^{16}O$, $H_2{}^{18}O$, and $HD^{16}O$, and they appear in relative abundance of 0.9977:0.0020:0.0003. Due to small differences in the properties of these isotopes, the physical processes of evaporation and condensation can change the isotopic composition of the atmospheric water away from the oceanic abundance ratio. The slightly lower vapour pressure of the heavy isotopes causes them to evaporate less often and condensate more often than the lighter isotopes. The ensuing change in composition is dependent on both the distance from the source region and the temperature to which the δ-values to first order show a linear relation. This also means that latitude and height above sea level will decrease the δ-value. The variable of interest in ice core studies is the deviation of the isotopic ratios from a standard reference value, known as Standard Mean Ocean Water (SMOW). These are denoted δ^{18}O and δD, referring to the deviation in the fraction of ^{18}O to ^{16}O and D to H respectively, and are defined as

$$\delta = \frac{R_{\text{sample}} - R_{\text{SMOW}}}{R_{\text{SMOW}}} = \frac{R_{\text{sample}}}{R_{\text{SMOW}}} - 1. \tag{3.2}$$

Here R denotes the fraction of heavy to light isotopes. Since the isotopic composition is temperature dependant, the δ-values will show annual variations, and can be used for layer counting in areas with high precipitation rates. When the signal of annual variations has been reduced below the level of the measurement noise, due to diffusion and thinning, the δ-values may still be used to estimate average past atmospheric temperatures and climate conditions below this point.

Sea Salt: Quite a number of primary aerosols, especially those containing Na, Mg, K and Cl originates with sea salt, [Paterson and Cuffey, 2010]. Many of the species also has other natural sources, and the strength of these non sea salt sources can be calculated as $X_{\text{nss}} = X_{\text{tot}} - X_{\text{ss}}$, where X_{tot} is the total amount of the species in question, and X_{ss} is the part originating from sea salt. This part, X_{ss}, can be calculated from the level of Cl^- in the ice, by assuming that all Cl^- is from sea salt, and then use the ratio of Cl^- to the species in question found in standard sea water. From the ice core records sea salt is known to be enhanced in cold periods, [Kuramoto et al., 2011], and hence anti-correlated with δ^{18}O. Since sea salt components are related to the oceanic environment it has been proposed, that sea salt is incorporated into the atmosphere from sea sprays, and hence that increased levels should be due to increased wind speeds, but in this case the salt levels should decrease with the extend of sea ice coverage which seems not to be the case. Another theory suggests that surface tensions draws brine to the surface of newly formed sea ice, where it is incorporated into hoar-frost crystals that the wind can take to the ice sheets, Kjær [2010]; Paterson and Cuffey [2010]. Since sea salt is correlated to cold environments, it can also be used as a seasonal marker with peaks in the winter time.

Continental dust: Dust is simply micro particles picked up by the wind on the continents, and their composition reflects the types of rocks and soil found on those continents. In the

case of Greenland, the source region is central Asia. Most of these particles are insoluble mineral dust from silicate rocks, and may bring along impurities of Fe, Al and Si, but some of the dust may be Ca based in the form of soluble $CaCO_3$, $CaSO_4$ or apatite. The soluble dust can in general be detected by measuring the Ca^{2+} concentration, while an Abakus, (see section 4.1.2), may be used to simply count the number of insoluble dust particles. Any changes in dust concentrations may be due to changes in mobilization in the source area, changes in transport and wind patterns, fall out during transportation and differences in deposition processes. As an example of these effects, the dust signal was much larger during the ice ages, where the source regions was dried out, stronger wind scoured the landmasses, and glaciers increased the erosion. In general though, the insoluble dust is regularly deposited in the boreal spring, and can therefore also be used as a seasonal signal in layer counting. Dust may affect the climate in several ways, as it may scatter and absorb solar radiation, as well as change the properties of clouds, and change the radiation budged, [Kjær, 2010]. Dust in the form of e.g. $CaCO_3$ may also change the pH of the ice, by neutralizing the acids present, [Atkins and Jones, 2010].

Biogenic: Biogenic emissions contributes mainly with a few chemical species, especially sulphur compounds and ammonium, NH_4^+. The sulphur compounds is responsible for the most important acid in the ice, as H_2SO_4 formed by dissolution of SO_2 in water droplets in the atmosphere, [Cole-Dai, 2010], and methane-sulphonic acid (MSA). Both SO_2 and MSA can be produced by oxidation of dimethyl sulphide gas (DMS), which is emitted by living organisms in the surface of the oceans. Hence they are believed to show evidence of the marine biogenic signal of phytoplankton, and an increased signal is believed to indicate more active blooms. Acidic sulphate is therefore believed to come mainly from photochemical oxidation of these biogenically derived sulphur gases, which corresponds to a peak in concentration during the summer, [Moore et al., 1992; Paterson and Cuffey, 2010].

On the other hand NH_4^+ has been shown to correlate to land based emissions from both soil and vegetation, as well as biomass burning from wildfires [Fuhrer et al., 1996]. This also indicates that NH_4^+ is a proxy for a summer signal, when vegetation are wide spread on land, and higher temperatures may start forest fires. Other proxies of wildfire emissions are potassium, [Mahowald et al., 2008], and vanillic acid [Paterson and Cuffey, 2010].

Volcanic: The gaseous emissions from volcanoes consist primarily of water vapour, carbon dioxide and reduced sulphur compounds (mainly SO_2), nitrogen and halogen compounds, and most eruptions are associated with the release of large amounts of dust as well [Cole-Dai, 2010; Karlöf et al., 2000]. Dust however tends to settle out of the atmosphere by gravity both quickly and locally, and might therefore not show up as signals in ice cores. In the oxidizing atmosphere, the SO_2 from volcanic and other sources is converted to the chemically stable sulphuric acid H_2SO_4, and volcanic eruptions therefore contributes with large amounts of non sea salt SO_4^{3-}, [Paterson and Cuffey, 2010]. Once SO_2 has been converted to sulphuric acid, the later (being highly hygroscopic) forms aerosols in the form of $SO_4^{3-} \cdot H_2O$. It is most often the wash out by precipitation of these aerosols that is measured as volcanic signals in

ice cores, as both pH and conductivity is affected by large increases in the ionic content, see e.g. Hammer [1980]; Moore et al. [1992]. The sulphuric acid of volcanic origin in polar snow, is superimposed as clearly elevated levels on the relatively stable background of sulphuric acid (and other ionic compounds), from continuous sources, such as the biogenic emissions mentioned above. Volcanic activity can therefore be seen as layers of increased acidity in the ice, and these layers can be used as time markers, if the date and site of the eruption is known. Detection of volcanic signals in ice cores is most easily done by using the conductivity measurements of section 4.4.

Anthropogenic: In the last 50-100 years there has been a substantial increase in production levels of both SO_2 and NO_x gases from industrial processes, especially as a result of coal burning, and this has produced a clear signal of increased acidity in the Greenlandic firn. Elevated levels of black carbon (soot) produced by incomplete combustion can be found in the firn as well, spanning back to the start of the industrial revolution, but the level of black carbon has decreased since about 1910. Black carbon in snow may contribute to global warming, by increasing the absorption of solar energy.

CHAPTER

4 Continuous Flow Analysis and Electrical Properties of Ice

In the previous chapter, it was argued that ice cores can indeed be used as a climate archive of the past, and the information the different impurities can provide was briefly outlined. In order to use this information, measurements need to be done, and for that the Copenhagen continuous flow analysis (CFA) system was used. This chapter presents how ice cores are prepared for CFA measurements, and what the CFA system actually is. The focus will be on the techniques used for the detection of phosphate and pH, although the subject of measuring the conductivity of the ice is also treated.

4.1 CFA measurement methods

Flow analysis techniques were introduced into the field of chemical analysis in the middle of the last century, in an attempt aimed at mechanizing the tedious and time consuming sampling and monitoring processes in industrial plants, [Estela and Cerdá, 2005]. Since then the analytical techniques has evolved along with the systems used, but the aim in using these techniques are still the same. Together with some degree of mechanization, measurements based on flow analytical techniques reveal better precision, a higher analysis throughput and a reduction in sample contamination, as compared to manual sample-by-sample procedures, [Kaufmann et al., 2008; Rasmussen et al., 2005]. In the case of ice core measurements, this also translates into a higher spatial resolution.

The analysis of climatic signals in ice cores started out as a very time consuming process, where each core section was divided into discrete centimetre long samples before analysis. Each of these pieces wes then dedicated to individual analysis of a climatic signal, such as analysis of gases, water isotopes, dust, chemistry etc. If the analyte was prone to contamination, using these small pieces of sample required extensive decontamination and preparation before measurements were made, and this resulted in a substantial loss of the ice core mate-

rial to be analysed, [Bigler et al., 2011; Kaufmann et al., 2008].

The CFA system for ice cores is designed to measure ions in a continuous flow of water, created when melting the core. The system consists primarily of a melting unit situated in a freezer, [Bigler et al., 2011]. The melting unit continuously melts the ice, splitting it into two streams. The inner part, also known as the sample, goes to analysis while the outer part goes to waste to eliminate any contamination that could have been caused by handling the ice. Notice that only enough of the outer part of the ice core is removed to avoid contamination, in order to keep the amount of water for analysis as high as possible. Outside the freezer in normal room temperature is sample/standard valves, a debubbler and the measuring units. The sample flow from the melting device passes through a debubbler to remove any air bubbles from the water, in order to make the flow steady and reduce the noise on the measurements. The air content can be analysed for its isotopic composition. Next the sample flow is split to feed the various analytical modules (possibly through a filter to avoid dust in the detection line) where it will most likely be mixed with reagents that allow for fluorescent or absorbent complexes to form, although other detection methods are available. As an example, the electrolytic conductivity and dust content can be measured directly in the sample stream. If fluorescent or absorbent techniques are used, which is the case for the measurements of this thesis, the amount of the complexes formed can be measured with spectrophotometric detectors. In order to convert the detector signal into concentration values however, ultra pure water (a blank) is passed through the system both before and after the sample has been processed in order to establish a baseline. Standard solutions of known concentrations of the chemical that is being measured, are processed at regular intervals in order to know how the system responds to various concentration levels, and this is used to construct the calibration curve, [Rasmussen et al., 2005]. In the case of phosphate and pH, the detection is based on absorbent techniques, see section 4.1.2. The techniques are optimized for low flow rates, because of the small quantities of ice available.

4.1.1 Preparation and melting of the ice

When drilled, the typical length of an ice core section is close to three meters, and depending on the setup used, has a diameter of 7 - 10 cm, [Kjær, 2010]. Each piece is then cut to a length of 55 cm for transportation purposes. When prepared for analysis, the core is cut into multiple pieces along the longitudinal axis, used for measuring different proxies. An example of a cutting plan can be found in figure 5, which represents the cutting plan used for the NorthGRIP ice core. This means that the CFA laboratory only gets part of the ice core, usually cut to the specified dimensions 35 mm x 35 mm, [Bigler et al., 2011]. Common to all cutting plans, is that the CFA part of the ice core is always an internal piece, in order to avoid contamination from handling the surface of the core. The NEGIS core was drilled in a dry borehole, and hence there is no risk of drill liquid contaminating the samples.

Further measurements to avoid contamination is made by removing any breaks in the ice

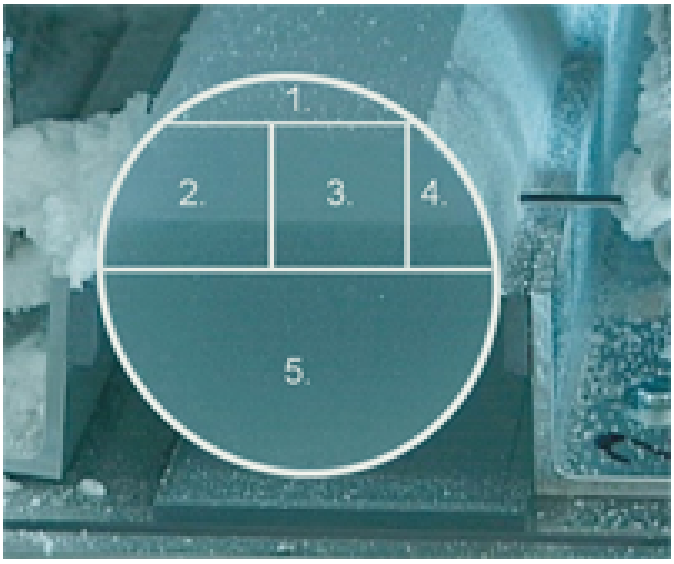

Figure 5: Cutting plan for the NorthGRIP ice core. The following are measured on the indicated core pieces: The physical properties of the ice (1), the gas content of the ice (2), impurities (3), stable isotopes (4), and electrical conductivity (5). After measuring the conductivity piece 5 is stored in the freezer at the Centre for Ice and Climate in Copenhagen for archive purposes. The figure is from [Centre for Ice and Climate, 2013b].

core sample. Both the ends of the ice core sample and any break may be contaminated e.g. by dust. For the NEGIS shallow ice core this was done using a band saw, and removing approximately 0.5 cm to each side of the break, and of the ends. The exact amount removed was measured in order to recreate the correct depth scale for the data. The importance of the filter may be realized by noticing, that as mentioned in section 2.1.1, a lot of nonsoluble phosphate is associated with dust, and if the dust is not removed by the filter, some of it may be dissolved in the acidic environment of the phosphate reagent and buffer, and it would be impossible to measure the concentration of dissolved reactive phosphorus directly. When the ice cores has been prepared and logged in the freezer, they are transferred to the CFA laboratory for processing. The CFA melting system is located in a small freezer that allows for the storage of several ice core samples, while measurements are proceeding. When melting the cores, a small cube of highly de-ionised ice prepared from milli-Q water, is placed at the melter before the ice core. This is done in order the make the transition from water to sample as smooth as possible. Milli-Q water is purified water from a milli-Q system (Millipore Corporation, MQ advantage A10, 18.2 MΩ/cm). In figure 6 the setup for the phosphate line of the CFA system is shown.

When processing an ice core, it is placed vertically on the melt head, and is pressed down by its own weight, as well as by an encoder used to measure to melt speed from which the

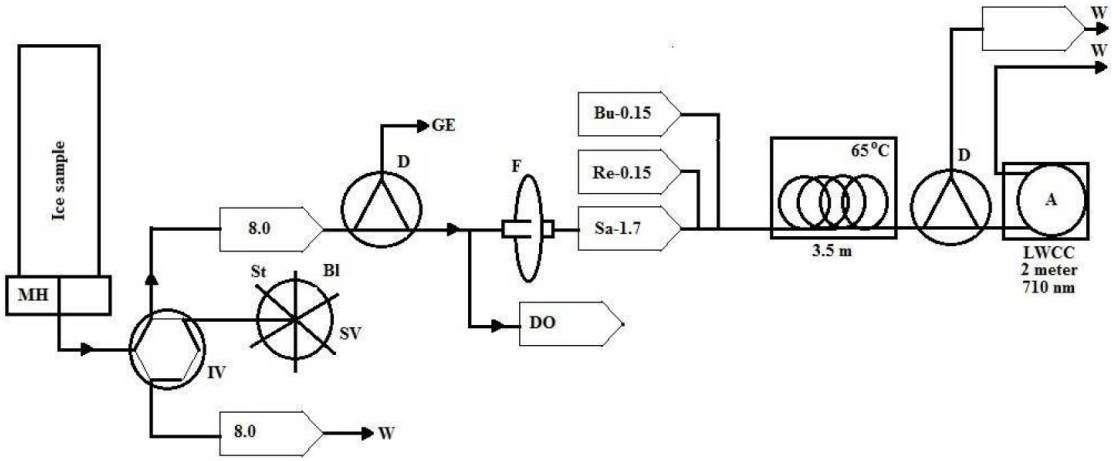

Figure 6: The continuous flow setup used for detection of dissolved reactive phosphorus. Ice is melted on a melt head (MH) in a freezer kept at -20°C. An injection valve (IV) in combination with a selection valve (SV) for standards (St) and blank (Bl) allows for running either. The sample line is de-bubbled (D) and the gas (GE) can be used for gas extraction measurements. The water line is split into various analytical channels (DO), and the PO_4^{3-} line which is the only one shown here. The water is filtered (F) to avoid interferences and the sample (Sa) is mixed with reagent (Re) and buffer (Bu) and then passed through a 3.5 m heated (65°C) mixing coil before a second debubbler (D) removes any remaining air. Absorption (A) at 710 nm is measured in a 2 m Liquid Waveguide Capillary Cell (LWCC) after which the line goes to waste (W). Numbers indicate flow rates in mL/min. The figure is from [Kjær et al., 2012a]

depth scale can be reconstructed. The melt head provides a chemically non reactive surface to melt the ice, which can be provided by many different materials. The Copenhagen CFA melt head is made of aluminium. It is designed to minimize mixing before sample analysis, [Bigler et al., 2011]. A schematic overview of the melt head can be found in many articles, and an example is shown in figure 7.

In summary, the CFA setup is simply a laboratory setup that allows for continuous melting and analysis of ice cores, rather than using discrete sampling methods. The reduced handling and continuous nature of the measurements result in good resolution, high measurement speed as well as an elimination of time-consuming sample cleaning. Also, almost any analytical method can be used with the CFA system, as long as the water flow from one of the detection lines is sufficient for the technique. Some of the techniques used with this type of system is described by Estela and Cerdá [2005], and examples are optical techniques, fluorescence spectrophotometry, chemiluminiscence photometry, atomic spectroscopic techniques, potentiometry, voltammetry, amperometry as well as ion chromatography, gas measurements and inductively coupled plasma mass spectrometry (ICP-MS). The techniques used for both phosphate and pH detection in this project, was absorption. The details of the specific setup used in this thesis can be found in section 4.3.

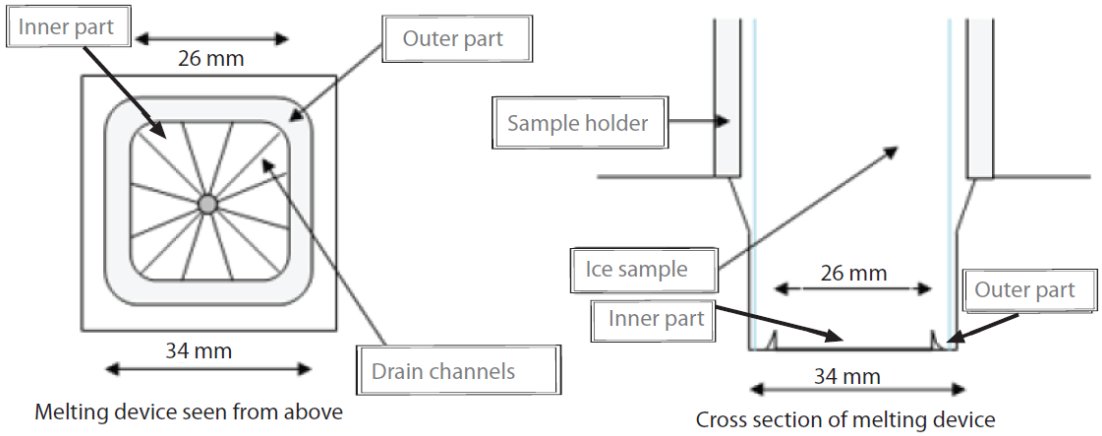

Figure 7: Schematics of the melting devices used in the Copenhagen CFA device, illustrating the concept of an inner and an outer part of the melt head. The figure is from [Kjær, 2010]

4.1.2 Detection methods

In this section, the principles of the methods used for detection will be explained. Absorption was used to detect phosphate, pH and Na^+ and fluorescence was used to detect NH_4^+, while the number of dust particles was simply counted using an Abakus. Given that the measurement of phosphate and pH was the main object of this thesis, emphasis is put on the absorption detection method.

Absorption: Different materials and molecules will absorb electromagnetic radiation to different extents at different frequencies. This knowledge can be used for measuring the fluid concentration of a chemical species, as the amount present in the solution will affect the degree of absorption. Hence all absorption detection methods depend on the absorption of light in the medium. In order to utilize this, the fluid is led into a waveguide of known length, ℓ. The intensity of the transmitted light, I, is then measured, and compared to the intensity of the incident light, I_0.

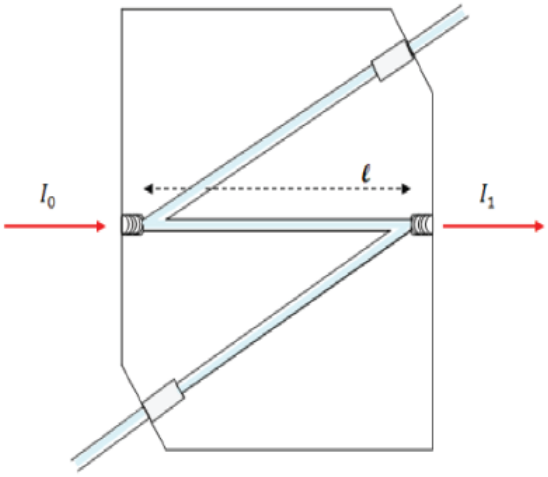

Figure 8: Example of a short flow cell of optical length ℓ. The figure is from [Kjær, 2010].

An example of an absorption cell can be found in figure 8. The relation of the absorption of light to the properties of the material, through which the light is travelling, is known as the Lambert–Beer law. This law states that there is a logarithmic dependence between the transmission of the light through the cell, and the product of the absorption coefficient of the substance, α, and the distance the light travels. The absorption coefficient can further be expressed in terms of the extinction coefficient, ε, and the molar concentration, c, of the absorbing species. In formulaic notation the relation is

$$A = \alpha \cdot \varepsilon \cdot \ell \cdot c = -\log_{10}\left(\frac{I}{I_0}\right), \tag{4.1}$$

which is actually just Abs = a·Conc + b, where Conc is the concentration, and Abs is the absorbance. This in turn can be rewritten to give the intensity of the signal

$$I(\ell) = I_0 \cdot 10^{-\alpha \cdot \varepsilon \cdot \ell \cdot c}. \tag{4.2}$$

From this expression it appears, that an increase in the length of the waveguide cell will result in a better limit of detection (LOD). However there are limits as to how long the cell can be made before other problems emerge, se section 4.3. Furthermore, the combined factor $\alpha \cdot \varepsilon \cdot \ell$ can be calculated using standard solutions of known concentrations, and by calculating back from the measured intensity of the transmitted light, it is possible to find the concentration of the analyte in any given sample. Naturally the concentration of the standard solutions should be of approximately the same strength as the sample in order to arrive at an accurate estimate of the sample concentration.

It should be noted, that the linear expression of equation (4.1) tends to break down at very high concentrations, where the molecules may be so close together, that they begin to interact. This may alter the extinction coefficient and cause the fit to be nonlinear. This effect can be seen when processing the standard solutions, but it did not occur during sample measurements due to low concentrations.

Fluorescence: Fluorescence is like absorption, a method that depends on the analytes ability to interact with light. If the molecule is excited by absorption of the incoming light, it will decay to its ground state again at a later time. The decay will emit a new photon, at the same, or at lower, energy than the original photon used for excitation. This emission is called fluorescence. If the decay channel utilizes a different wavelength than the absorbed light, it will be quite easy to distinguish the signals, and measure the strength of the fluorescence signal only by using an optical filter.

Mineral dust: As mentioned in section 3.4, mineral dust is simply the insoluble part of continental dust, meaning that the abundance is found simply by counting their numbers, and in some systems their size as well, using an Abakus. The water going to the Abakus has to pass through a narrow slit that should be wide enough to let only one dust particle through at a time. This passing of dust particles then breaks a signal created by a laser mounted orthogonal to the stream. To convert the unit of counts per second to counts per centimetre ice

core, it is necessary to know the flow rate through the cell. Hence the Abakus is mounted in line with a flow counter.

Conductivity: The liquid conductivity is simply the measure of electrolytic conductivity, the ability for the fluid to conduct an electric signal, and is hence a measure of the bulk signal of the major ions. As mentioned in section 3.4, it is also used to detect volcanic signals, due to the increased level of sulphuric acid associated with eruptions.

4.2 Treatment of CFA data

When the raw data has been obtained from ice core measurements, the signal can seem quite erratic, and some enhancements is in order. This can be done simply by smoothing the signal, if accumulation rates at the drill site, and hence the resolution, is good. However, when analyzing the deeper sections of ice cores or cores from low-accumulation areas, there may be a need for further improvement of the resolution. This can be done by deconvoluting the signal, as described by Rasmussen et al. [2005]. Deconvolution is the assessment of the degree of mixing and therefore smoothing that occurs in the system, in order to counteract the effect. If the approach of deconvolution is to be used, the step function used in the process can be obtained from the standard solution calibrations, but in this case both the blank-standard and standard-blank response should be measured, instead of measuring only the standard-standard response, as was done for this thesis. For this thesis the NEGIS shallow core was analysed, and for that the temporal resolution was good to start with, so the simple approach of smoothing was used.

Examples of raw and smoothed data can be found in the calibration curves shown in the next chapter.

4.3 CFA systems used in this thesis

For this thesis, the setup used to detect dissolved reactive phosphorus is the method developed by Kjær [2010], and is based on a standard molybdenum blue method. The details of the setup will be described here, along with the setup used for pH measurements.

The NEGIS firn/ ice core was processed at the Centre for Ice and Climate in Copenhagen. Density measurements, section 5, and electrical properties, section 4.4, was measured prior to the actual CFA measurements, and the cores were cut into a 35 mm × 35 mm × 55 cm bars with a band saw. The CFA setup used for phosphate can be found tabulated in table 3, and the schematics can be found in figure 6. The melt head was made of aluminium, and was kept at a temperature at around 35°C, but was adjusted when needed in order to keep a melting rate of about the 5 cm/minute in the firn part of the core, while a melt rate of about 4 cm/minute was used on dense firn and ice. These melt rates were needed to feed all the detection lines. The melt rate (cm/min) was measured using a encoder. The melt water

was sent through a polymer debubbler before being divided between the lines: stable water isotope ratios, electrolytic conductivity, ammonium, sodium, pH, insoluble dust and a phosphate line. The dust line went through an Abakus combined with a flow counter to find the amount of dust as counts/mL. The debubbler had been optimized to ensure minimal mixing of the sample before analysis. Blanks and calibration standards, section 5.1.1, was measured approximately three times (start, middle and end) on each day of analysis, on which about 7 meters of firn/ice was melted.

The methods chosen for analysis must be able to meet the constraints set by using the CFA system, and be able to complete the measurements at the same rate the sample is produced. Furthermore, previous analysis of ice cores show very low concentrations of phosphate in the order of 0.25 ppb [Edwards et al., 2007] to 0.32 ppb [Kjær, 2010], and hence the chosen method should be sensitive enough to allow for such low concentrations. As mentioned in section 4.1.1, quite a number of analytical setups can be used with the CFA system, but not all of them are easy to implement. Kjær [2010] therefore settled on spectrophotometric methods, because of their ease of use in the CFA setup and potentially high accuracy, [Estela and Cerdá, 2005].

The spectrophotometric method for phosphate uses molybdate for detection, as orthophosphate reacts with molybdate under the influence of ascorbic acid to form a clear blue liquid known as 12PM or 12-phosphomolybdate blue, equation (4.3), [Kjær, 2010], which makes the absorption of red light, in the range 660 nm to 885 nm, dependant on the phosphate concentration. Information on this method can be found in [Estela and Cerdá, 2005].

$$PO_4^{3-} + 12MoO_4^{2-} + 27H^+ \rightarrow H_3PO_4(MoO_3)_{12} + 12H_2O. \tag{4.3}$$

An LED light source with a wavelength of 710 nm was used for measurements. The absorption of red light happens in accordance with the Lambert-Beer law as described in section 4.1.2. To stabilize the reaction antimony tartrate that acts as a catalyst was used, [Estela and Cerdá, 2005; Kjær, 2010], although many alternatives for both ascorbic acid buffer and catalyst exists.

The molybdenum blue method normally exhibits a LOD of about 2.85 ppb PO_4^{3-}, [Kjær, 2010], which is somewhat above the estimated concentration in ice of 0.25 ppb, but there are ways to get around this by enhancing the signal. The normal ways of enhancing a signal in chemistry includes doing preconcentrations, [Estela and Cerdá, 2005], i.e. concentrating the sample prior to measurements, optimizing of the chemistry, and in the case of absorption signals, lengthening the cell. Due to the nature of the CFA setup, doing preconcentrations is not feasible, though some excellent results have been achieved with the technique, with LODs in the ppt range, [Estela and Cerdá, 2005]. If very accurate measurements are needed in a small depth interval of the ice core, doing preconcentrations on discrete samples may be a good solution. Likewise, from the literature, [Kjær, 2010; Pasteris et al., 2012], the chemistry of the setup would seem to have been optimized as far as possible.

From the Lambert-Beer law it appears that the concentration of the solution is inversely proportional to the length of cell, end hence lengthening the cell will reduce the LOD. Unlike the other two signal enhancing approaches, lengthening the flow cell is quite easy, but of cause this cannot be done indefinitely. Kjær [2010] found that for mixing lengths of less than 2 meters, small air bubbles would form in the flow path, which upon entering the flow cell would result in anomalous signal absorption. If the waveguide was lengthened, the backpressure would increase and prevent these micro bubbles from forming, but at the same time provide a larger surface area for any stray dust particles or air bubbles not removed by the filter and debubbler to get stuck.

Dust particles may have a large capacity for absorbing phosphate from freshwater solutions, [Paytan and McLaughlin, 2007], and any dust stuck in the flow cell may change the phosphorus concentration of the solution, at least until the dust has been saturated. Dust/air bubbles might also refract the incident light or block it altogether. To avoid particulates in the flow cell, as well as to ensure that only water soluble phosphate was detected, a 0.2 μm filter was installed before the introduction of reagents in the sample. Furthermore, the linear range of detection also decreases with the length of the flow cell, and in the end a 2 m long waveguide capillary cell (LWCC) with a diameter of 0.5 mm was used. Using this approach, it has been shown that an LOD of (three times standard deviation) 0.049 ppb is possible, [Kjær, 2010], and this is well below the desired level.

	Flow rates:
Sample	1.7 mL/min
Reagent	0.15 mL/min
Buffer	0.15 mL/min
LWCC detector	1.8 mL/min
Debubbler waste	0.20 mL/min
Particle filter pore size	0.2 μm
Reagent mixing length	3.5 m
Reagent mixing temperature	65 °C
Absorption path length (LWCC)	200 cm
Absorption wavelength	710 nm
Spectrometer integration time	800 ms
Analytical uncertainty	1.1 nM (0.1 ppb)
Linear range	< 105 nM (10 ppb)
Response time (5 -95%)	18 s (<53 nM)
	40 s (>53 nM)

Table 3: DRP CFA detection system parameters.

Due to the overall charge of PO_4^{3-}, it has a tendency to stick to the side of glass bottles used for storing, [Kjær et al., 2011]. Hence all reagents were stored in polypropylene bottles to limit this effect. All reagents were of analytical grade from Merck (Darmstadt, Germany). The recipes for the reagents and buffers used can be found below.

Recently more CFA techniques for measuring pH directly in ice cores has been investigated by e.g. Pasteris et al. [2012] who has presented a method using a glass pH electrode, and Raghuraman et al. [2006] used a combination of dyes in a spectrophotometric method. Since the first approach has not been tested on alkaline ice so far, the later is used in an adapted version in this thesis. This method further has the advantage, as compared to an electrical pH probe, of increased sensitivity made possible by changing the flow path length, and by use of interchangeable dyes to fit e.g. more alkaline samples.

The setup used for the measurement of pH is based on Raghuraman et al. [2006], with an optimized dye mixture of two components. It is likewise an absorption method similar to that of PO_4^{3-}, but the concentrations of acidic elements in the ice is much higher than the concentration of phospahte, and hence a smaller flow cell of 5 cm of the form seen in figure 8 was used. The reagents were bromophenol blue and chlorophenol red in aqueous solution, and the melt water/reagent mixture were heated to 65°C to increase the reaction rate. Two different wavelengths, 586.35 nm and 589.76 nm, was used for absorption.

Molybdate reagent recipe:

1. Dissolve 0.74 g ammonium molybdate in 50 mL 5N H_2SO_4.
2. Add 10 mL of stock antimony potassium tartrate.
3. Dilute the mixture in 100 mL milli-Q water.

The **stock antimony potassium tartrate** is made by dissolving 0.3 g antimony tartrate in 100 mL milli-Q water, and it is kept in a dark bottle at temperatures below 4°C, to improve its lifetime.

Ascorbic acid buffer:

1. Dissolve 0.5 g ascorbic acid in 100 mL milli-Q water.
2. Add 7 g sodium dodecyl sulphate,

while the **pH reagent** was prepared by dissolving 0.025 g bromophenol blue and 0.025 chlorophenol red in 500 mL milli-Q water.

Besides measuring PO_4^{3-} and pH, the CFA system used also measured the mass concentration of water-soluble sodium (Na^+), ammonium (NH_4^+), the electrolytic melt water conductivity (σ) and the number of insoluble dust particles (dust). To first order, this means that the system provided proxies of marine (Na^+), terrestrial (dust) and biogenic (NH_4^+) environments, while the conductivity is a sum parameter of all ionic constituents in the ice.

4.4 Electrical properties of ice

As mentioned in the introductory chapter of this thesis, the NEGIS shallow core was processed to construct both a density profile and electrical conductivity profiles some time before the CFA measurements were conducted. Hence these measurements is not related to the CFA setup, but are included here for completeness.

Previously high resolution continuous detection of acidity in ice cores has mainly been done by using electrical conductivity measurements (ECM), and DiElectric Profiling (DEP) along with calculations of the ion balance, [Pasteris et al., 2012]. These techniques measure the electrical properties of ice rather than the acidity directly, but has the advantage, that a better understanding of the factors that determine the electrical properties of ice also helps improve interpretation of radar soundings in ice sheets, [Wolff, 2000]. The electrical properties is directly related to the ionic content of the ice that is provided by chemical impurities, [Cole-Dai, 2010]. ECM is a DC method developed by Hammer [1980], which is highly dependent on the H^+ concentration, and has been used as an indicator of acidity in ice. The method has proven particularly useful in defining volcanic reference horizons, [Hammer, 1980]. DEP on the other hand is an AC method, [Moore et al., 1992, 1994], and the electrical signal has been shown to depend on both acid and salt content of the ice, [Moore et al., 1992; Wolff, 2000]. The difference stems from salts giving rise to Bjerrum defects, which are effectively bound charges, that cannot contribute to a DC current, but do produce AC conductivity.

Even though ECM and DEP has been widely used as indicators of acidity levels in ice cores, the ECM fails for alkaline or very weakly acidic samples because the conductivity goes to zero, [Moore et al., 1992]. The strength of the conductivity measurements lies instead in their ease and speed of use, as well as being nearly non-destructive, [Hammer, 1980]. The current measured by ECM can be converted to H^+ concentration by using an empirical calibration curve. While the calibration curve for DEP measurements varies linearly with the salt and acid content of the ice, [Moore et al., 1992], an ECM calibration curve has been proposed by Hammer [1980] to be of the form

$$H^+ = 0.045 \cdot I^{1.73}, \tag{4.4}$$

but evidence seems to suggest, that the parameters of this formula may depend on the physical properties of the ice, such as the intracrystalline structure and grain-boundary conduction, [Moore et al., 1992, 1994; Sugiyama et al., 2000], although these differences may also relate to the chemistry or the method used. Different formulas are proposed by Moore et al. [1992]. Also these formulas were arrived at while measuring deep ice cores, and hence the result may turn out to be unsuitable for use on a shallow ice core. It has been suggested that the ECM current should, in this case, be scaled by the relative density of the firn as compared to ice, in order to account for the larger amount of air in the firn ice [Kjær, 2013], and in this case, the calibration curve would be of the form

$$H^+ = c_1 + c_2 \cdot \left(\frac{I}{\rho_{\text{rel}}}\right)^{c_3}, \tag{4.5}$$

where c_1, c_2 and c_3 are constant parameters, that may be tuned to fit the calibration curve of the present drill site, and ρ_{rel} is the relative density of the firn, that is the density of the firn being measured as compared to the density of glacial ice which is 917 kg/m^3. Other approaches to density corrections has been addressed by Barnes et al. [2002], who fitted data and volume fractions of firn to ice from the top 300 meters of the Dome C core from Antarctica, in order to investigate different models of conductivity in ice. It is interesting to note that their approach to the percolation model of conduction is very similar to what was proposed in equation (4.5), but they proposed other lines of attack as well. The percolation model attributes the conductive properties of ice cores to liquid impurities held outside individual grains of ice. Each grain is then considered as a site in a conducting lattice, and electrical transport takes place on the surface of ice crystals. Barnes et al. [2002] notes that this model is reasonable for polar firn, where the presence of air bubbles and networks could easily provide a structure where a film of liquid impurities covering the grains could provide for conduction to occur. Barnes et al. [2002] found that ECM current could be density corrected by

$$\sigma_{\text{DC}}(v) = \sigma_{\text{DC}}(1)1.23(v - 0.075)^{2.7}, \tag{4.6}$$

where v is the volume fraction. This approach was tried, and the result was very much comparable to the result of equation (4.5), but did not manage noticably better. Like ECM the DEP data has been scaled by the density fraction in this thesis, but only to the first power. The result of these corrections can be seen in figure 22 in section 6.4. Even though the density corrections is important in the firn layer, the controlling parameter is still by far the chemical content, [Wolff, 2000]. Even so, the necessity of the ad hoc density corrections made to equation (4.4) makes it difficult to trust the predicted acidity, but in the case of the NEGIS core the estimate made by equation (4.5) is certainly better than the original proposal by Hammer [1980]. This further has the side effect, that it is not possible to explore the CO_2 acidity calibration issue based on the ECM and DEP measurements, and since ECM is the only conductivity measurement performed on the NEGIS core, besides direct pH measurements, that measures the pH, it was not possible to explore the CO_2 calibration issues further than a literature study, see section 5.1.1. It is possible that performing these measurements on a section of a deep ice core, where no density corrections are needed, would give a better understanding of the effect of different concentrations of CO_2 in the ice would have on acidity.

If the methods of ECM and DEP are used to detect volcanic signals as mentioned in section 3.4, this is done on the assumption that the acid content of the ice is the most important contributor to the electric conductivity of ice, and that any brief elevation in level of the acidity is caused by the input of volcanic sulphuric acid, [Hammer, 1980]. This assumption however, may not be that accurate after all. The presence of other acids in the ice, the variability in the background sulphuric acid signal and the neutralization of volcanic acids by alkaline dust may change the conductive properties of the ice. Besides the changes in conductivity

caused by the chemical content (other than sulphuric acid) of the ice, the temperature and the physical properties also have an effect, [Cole-Dai, 2010; Moore et al., 1992]. All of these complications limit the quality of the volcanic record of the ice from these conductivity measurements. In general only major eruptions leave clearly visible layers in the ice.

Furthermore the liquid electrolytic conductivity cannot necessarily be compared directly to neither ECM nor DEP. The reason for this is that both of these techniques measure the properties of ice, while the chemistry is measured in the melted sample. During the melting process soluble particles will be dissolved. These particles is likely to have only a limited effect on the electrical properties of the ice, but may influence the chemistry in water significantly, [Taylor et al., 1992]. The relationship between the different measurement techniques is explored further in section 6.4.

CHAPTER

5 The NEGIS Shallow Ice Core

The North Eastern Greenland Ice Stream (NEGIS) is Greenland's largest ice stream with a length of approximately 1000 km, beginning at the ice divide, and it reaches velocities of as much as 100 m/yr. Hence it is an important piece of the Greenland ice sheet mass balance. The topography of the area has been studied with satellite radar interferometry and radio echo measurements. As mentioned in the introductory chapter of this thesis, the NEGIS shallow ice core is a dry borehole firn core from Greenland, 75.623°N, 35.96°W, that was retrieved during the 2012 NEEM field season. It has a length of approximately 70 meters, and covers the years 1607 to 2012. The firn/ice part covered 66 meters, and this part was cut into a total of 115 bags of 55 cm in length for transportation and subsequent analysis. CFA measurements conducted were dust particle concentration, electrolytic conductivity, sodium, ammonium and phosphate concentration as well as pH measurements. Annual cycles were observed for all parameters, which made a seasonally resolved chronology for the entire core possible, and volcanic markers were used as reference points. A list of volcanic signals detected can be found in table 7. In figure 9, the measured density profile and layer thickness are shown. The density profile was obtained by weighing samples of known volume, while the layer thickness was determined from layer counting. In this chapter a presentation of the data processing techniques used on the data obtained from measurements of the NEGIS shallow core is presented, using the setup of chapter 4.

5.1 Calibrations

As mentioned in section 4.1, in order to use the data obtained from the CFA measurements, it is necessary to know how the setup responds to different concentrations of the impurity in question. For this purpose standard solutions of known concentrations was processed several times a day, with a maximum of 6 ice core samples processed in between standards.

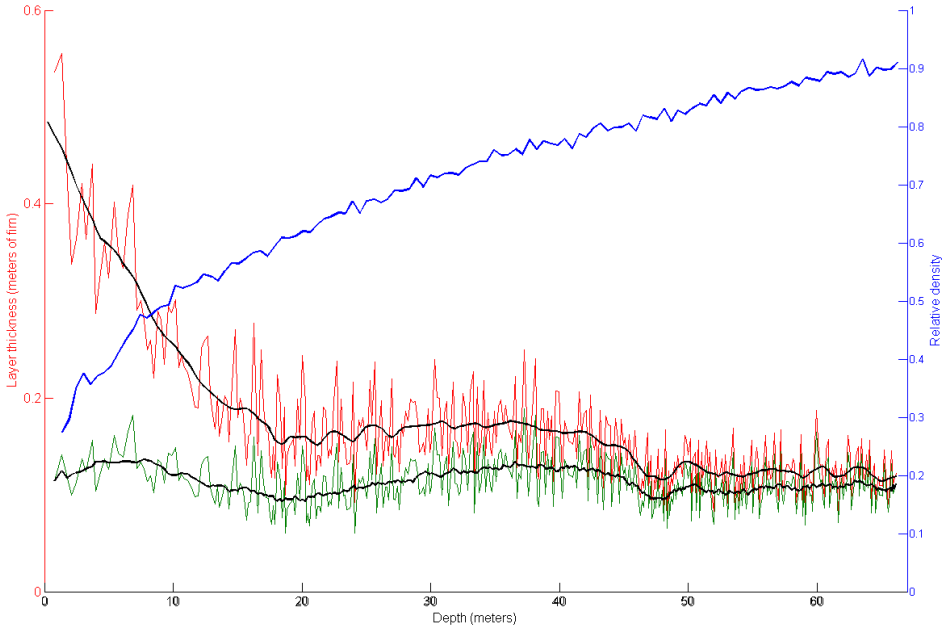

Figure 9: Information regarding the NEGIS firn core. The blue curve is the measured firn to ice density ratio. The red curve is the layer thickness in meters, and the green curve is the layer thickness in meters of ice equivalents calculated from the other two. The black curves are smoothed versions of last two.

Standard solutions was processed for all chemical species the CFA setup was measuring, including the pH and PO_4^{3-}.

5.1.1 Standards

The concentration of a series of diluted solutions can be calculated iteratively using equation (5.1). Here C_{n+1} is the concentration of the new solution, C_n is the concentration of the original solution and V_n and V_{sol} are the volumes of C_n and solvent used respectively.

$$C_{n+1} = \frac{C_n \cdot V_n}{V_n + V_{\text{sol}}}. \tag{5.1}$$

Standard solutions were obtained using this iterative approach on analytical grade solutions. The resulting concentrations can be found in table 4 for both PO_4^{3-} and pH. The uncertainties stated are based on the precision of the pipettes used to measure the volumes. Two different pipettes were used for this. One measured volumes in the order of 100-1000 μL, and for this pipette the inaccuracy ($< \pm 0.5\%$ to $< \pm 0.7\%$ depending on the volume) and the imprecision ($< \pm 0.2\%$ to $< \pm 0.5\%$) was stated in the technical information of the product. The largest uncertainties stated are for the lowest volumes and vice versa. The second pipette that was used

PO_4^{3-} standard	milli-Q	Org. conc.	PO_4^{3-}	Conc.	Conc.	Uncertainty
Unit:	mL	ppb	mL	nM	ppb	ppb
dil. 1	50	999000	0.5	104150	9891.09	121.96
dil. 2	50	9891	1.0	2042	193.94	3.23
ST 1	50	193.94	2.0	78.5	7.46	0.27
ST 2	50	193.94	1.0	40.0	3.80	0.14
ST 3	50	193.94	0.5	20.0	1.92	0.07
ST 4	50	193.94	0.2	8.1	0.77	0.03
ST 5	50	193.94	0.1	4.1	0.39	0.014

pH standard	milli-Q	Org. conc.	pH	Conc.	Conc.	Uncertainty
Unit:	mL	mM	mL	μM	ppm	ppm
HCl dil. 1	60	100.1	0.6	991.09	36.14	0.761
NaOH dil. 1	60	100.2	0.6	992.07	39.68	0.786
HCl 1	60	0.991	1.2	19.43	0.709	0.021
HCl 2	60	0.991	0.6	9.81	0.358	0.011
HCl 3	60	0.991	0.3	4.93	0.180	0.005
NaOH 1	60	0.992	1.2	19.45	0.778	0.022
NaOH 2	60	0.992	0.6	9.82	0.393	0.011

Table 4: Concentrations and uncertainties on the pH and PO_4^{3-} standard solutions. The milli-Q column represents the amount of water used to dilute the solution in question, which had the original concentration (org.conc.) seen in column three, and was used in the amount noted in column four. The resulting concentrations and uncertainties are found in the last three columns. Notice that the PO_4^{3-} data is listed in units of ppb, while the acidity components are in ppm.

measured volumes in the order of ~50 mL, and for this the uncertainty on measurements was estimated from double checking the measured volumes against a graduated cylinder. It was found to be in the order of 2% or 1 mL in 50 mL. The uncertainty on the analytical grade solutions was in the order of 0.2R%. The combined result follows from standard error propagation, and evaluates to just under 3%, depending on what interval of the fine pipette volume was used. Numbers can be found in table 4. This of cause is only the error on the concentration of the standards used. A review on further uncertainties associated with the measurements can be found in section 5.3.

As mentioned in section 4.1.1 the data series can be converted from a time measurement to a depth measurement, by using the encoder information, which provided the melting speed in cm/second. As mentioned in the same section, any breaks in the ice core sample, as well as both ends of the sample, may be contaminated by dust and other impurities. These parts were removed from the ice, and the breaks were inserted in the data series, before the cores were inserted at the correct depth scale.

PO_4^{3-} standards

The PO_4^{3-} standard solutions was prepared from a 999 ppm PO_4^{3-} solution of analytical grade from Merck (Darmstadt, Germany). This was diluted several times in order to give standard solution with concentrations that was comparable to what was expected from ice core measurements. As mentioned earlier, phosphate has a tendency to stick to the sides of its container. To limit this effect the standard solutions was kept in polypropylene bottles, and was processed as soon as they had been prepared, but this tendency still contribute to the uncertainty of the standard solution concentrations.

An example of a CFA measurement of one of these standard series can be found in figure 10, where both the raw data and the smoothed version can be found. The absorbance of the standard was found as the average value of measurements on each plateau, while the error associated with the absorption of the standard was found as the standard deviation on the same interval. The Lambert-Beer law, equation (4.1), is then used to obtain a linear fit to be used as the calibration curve, and a linear least squares approach was used to calculate the uncertainties on the slope and the intercept.

The calibration curve to the standard solutions of figure 10 can be found in figure 11. As mentioned in section 4.1.2 and 4.3 respectively, the higher concentrations may deviate from a straight line fit due to changes in the extinction coefficient, or phosphate being stuck on the sides of the bottle. Based on the observed data, the first effect seems most pronounced, since the absorption is higher than would be expected from the fit to the weakest standards alone. To test how well a straight line fits the data, one can calculate the coefficient of determination, R^2, or the probability of finding a poorer fit from a χ^2 calculation. In figure 11 the probability of the fit using only the lowest three standards as well as by using all five standards is shown. They are found to be 0.781 and 0.063 respectively. This shows the general trend for all standard solution series conducted for phosphate in this thesis: the fit using only the lowest three standards is much better than using all five, although a probability of 0.06 cannot be rejected outright. Given that the concentrations of phosphate to be found in the ice core is of the same order of magnitude as those of the weakest standards and that this was the case for the entire NEGIS core, it was decided that the fit using only the weakest three standards was used preferentially to construct the calibration curves.

From the calibration curve obtained above, and as can be seen in figure 11, the intercept does not actually correspond to phosphate not being present. As the intercept is simply the absorption of pure milli-Q water, this should have been the case. Therefore one further fit was made, forcing the intercept through the zero point, and the likelihood of this fit was calculated as well. In the case of the above fit, it was found to be 0.323, and hence the fit was a little poorer than using only the weakest three standards but all calculations has been done using these forcing fits as well. An explanation of the difference between the two fits used could be that the weaker the standard in question was, the larger a fraction of the phosphate present would be stuck on the sides of the container bottles lowering the concentration, and

hence forcing the intercept downwards. This effect could possibly be examined by measuring the concentration of the standards with more precise methods, prior to running them as standards, but this effect has not been investigated further in this thesis.

Furthermore there was some ambiguity as to how the baseline, I_0, should be chosen, and therefore the absorption for phosphate was calculated using equation 4.1 based on more than one baseline. The baseline could be calculated by averaging a few minutes of blank (milli-Q water) that could be assumed to be essentially free of phosphate, and the standard deviation on the baseline would simply be the standard deviation of the blank response signal. However, the baseline might also be chosen as the highest intensity response of the blank, since when using an absorption technique this would correspond to the most pure water and any lower values may simply have been caused by slight variations in the flow rate. Again the standard deviation was assumed equal to the standard deviation of the blank response signal. The signal for detection of a standard was found using the average intensity obtained during the detection of the standard, and the duration is the time between a 95% change in intensity since the previous standard, and a 5% change towards the next.

pH standards

The pH standard solutions were prepared by diluting a 0.1001 M HCl solution and a 0.1002 M NaOH solution, again from Merck, in order to account for the response to both acidic and alkaline ice. The standard solutions were processed in the same way as for phosphate to obtain the calibration curves. In the case of the pH, five standard solutions was prepared, and all five strength solutions were used to make the best fit for almost all calibration curves. However, on two out of the twelve days measurements was carried out, the alkaline solutions seemed to be much stronger than the solution should allow for. In figure 12 a typical response to a standard pH run is shown, while one of the off signals is shown in figure 13. As can be seen in table 4, the standards HCl 1 and NaOH 1 is very close to the same concentration (in μM), as is the case for HCl 2 and NaOH 2. The pH detection system should therefore give a response of about the same magnitude, but opposite in directions, for standards of the same concentration. From figure 13 it appears that this is not the case. Since the ice core samples is mostly acidic, only the three acidic standard solutions was used to make the calibration curves on the two days where the alkaline response signal was off. The cause of the sudden change in response to alkaline solutions, may have been caused by the use of an old reagent, or a slight contamination of the milli-Q water used to prepare the standards.

As mentioned in section 2.2, the ice core samples may be under saturated with respect to carbon dioxide immediately after melting, and this may cause the pH to drift. Pasteris et al. [2012, 2009] proposed a solution to this problem, based on equilibrating the sample with a known partial pressure of CO_2. This would produce pH measurements that would have almost no uncertainty in the CO_2 content, which makes it possible to calculate the concentration of hydrogen ions contributed by dissolved CO_2, and thereby adjust the measured

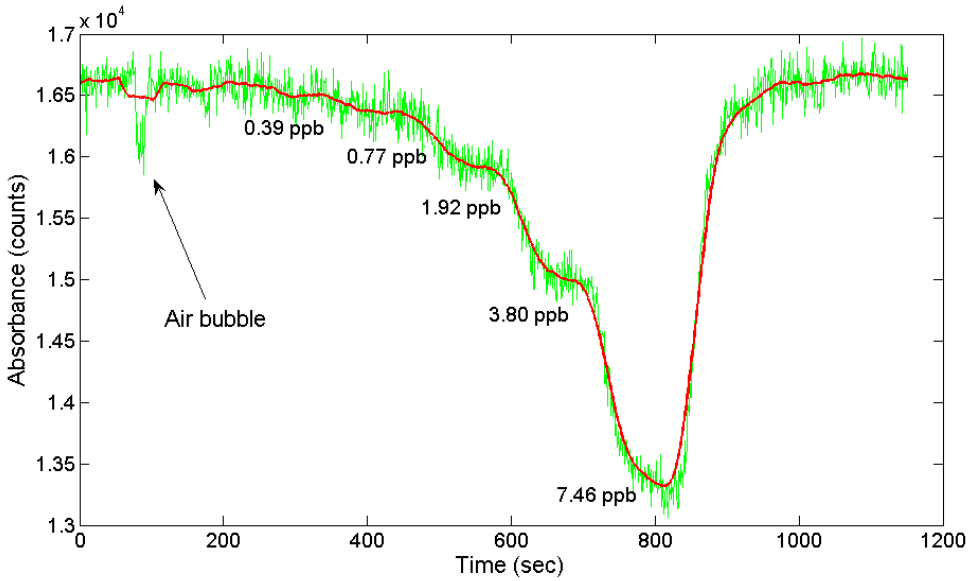

Figure 10: Standard run 1 from January 14. The green curve is the raw data, while the red curve is smoothed over 50 seconds, both is a function of the time since the start of the measurement. Two air bubbles can be seen before the first valve change.

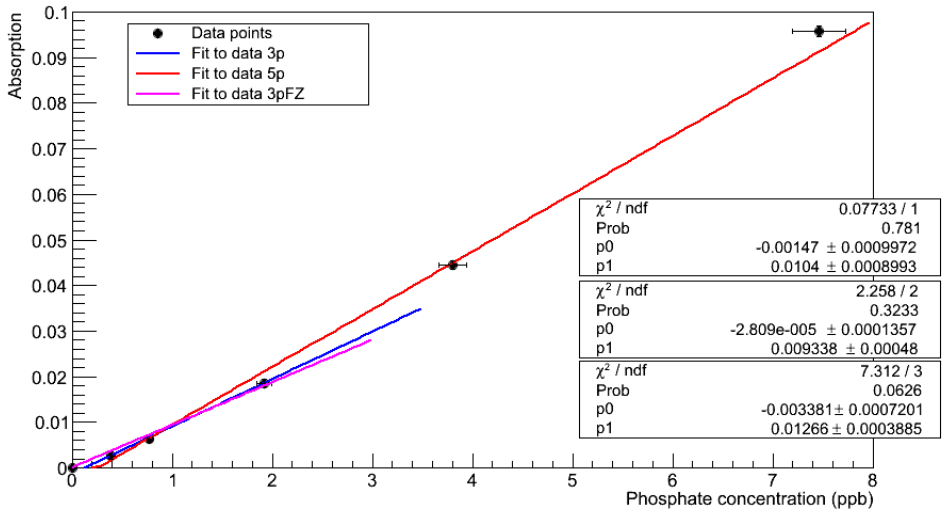

Figure 11: Calibration curve for Standard run 1 from January 14. The blue curve is the fit to the first three data points only (the lowest concentrations), while the red fits to all five data points and the magenta line uses the weakest three standards, and are forced through the zero point. Fit parameter information can be found in the boxes in the plot. All are linear fits, where p_0 is the intercept and p_1 is the slope, as stated in the figure.

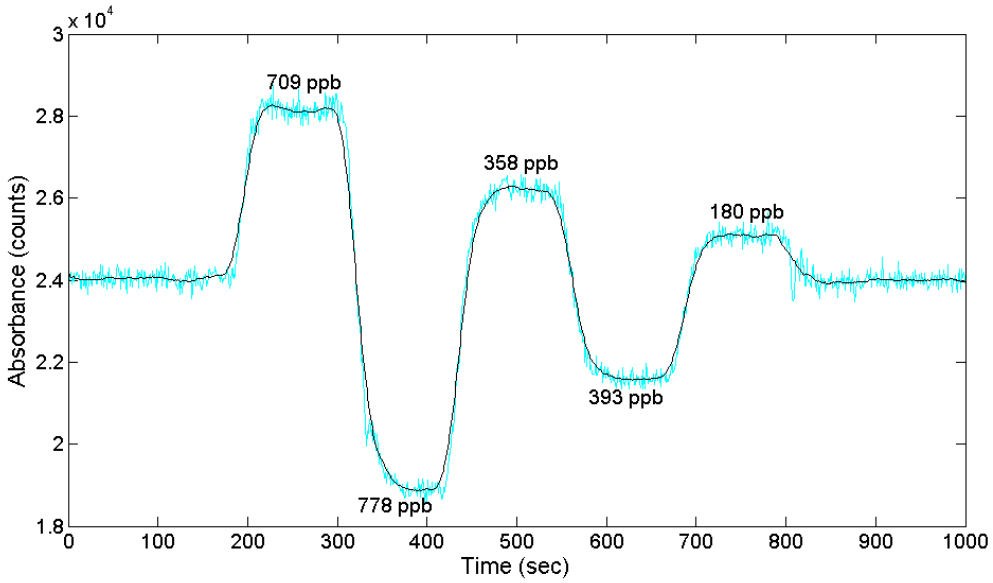

Figure 12: pH standard run 1 from January 15. The blue curve is the raw data, while the red curve is smoothed over 30 seconds. This is a normal looking (symmetric) response to the standards.

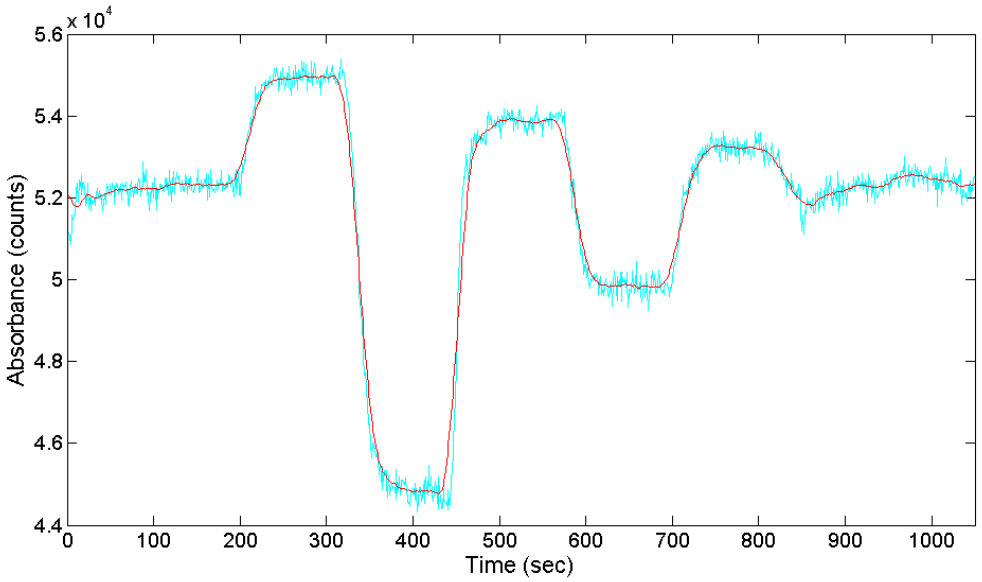

Figure 13: pH standard run 4 from January 28. The blue curve is the raw data, while the red curve is smoothed over 30 seconds. Here the contamination shows by skewing the curve.

pH according to equation (2.3). Unfortunately only an approximation to this setup was used when analysing the NEGIS shallow ice core, in that the sample was equilibrated only with the partial pressure of CO_2 in atmospheric air in the CFA laboratory. There the CO_2 concentration may have varied with the time of day, and the number of people present in the laboratory. Because of this, the partial pressure of CO_2 is not known exactly, and this will contribute to the error on the pH to acidity calculation, but should not affect the overall correlation to the other impurities in the ice. When calibrating, it was assumed that the partial CO_2 pressure was at a constant level of 450 ppm – a little higher than the atmospheric values due to human respiration – and that it has an associated uncertainty of 50 ppm.

The subject of calculating the concentration of hydrogen ions contributed by CO_2 can be dealt with by using Henry's law. This states that at a constant temperature, the amount of a given gas that can be dissolved in a given type and volume of liquid, is directly proportional to the partial pressure of that gas, in equilibrium with that fluid. That is to say, if the temperature, the pH and the partial pressure is known, then the CO_2 contribution can be calculated. This is done using equation (2.3), which can be rewritten in terms of the ionization fractions, α_0, α_1 and α_2, that for CO_2 in aqueous solution is fractions of H_2CO_3, HCO_3^- and CO_3^{2-}, [Pasteris et al., 2012, supporting information]:

$$\text{acidity} = \left[H^+\right] - \frac{K_H P_{CO_2}}{\alpha_0}(\alpha_1 + 2\alpha_2) - \frac{K_w}{\left[H^+\right]}. \tag{5.2}$$

The ionization constants are functions of the dissociation constants, K_a, and the pH. The relationship is given explicitly in the section Acidity equations of the appendix.

Neither the temperature nor the partial CO_2 pressure at which the solution was equilibrated is known exactly. The solution was heated in a heat bath to a temperature of 65°C, and it is assumed that the solution was likewise given plenty of time to reach the equilibrium, but measurements were not conducted to confirm this. The partial CO_2 pressure was not measured, but from measurements of common office concentrations, the concentration is assumed to be quite variable. For this reason a value of $P_{CO_2} = (450 \pm 50)$ ppm was used. The value is somewhat higher than the atmospheric CO_2 partial pressure due to the number of people working in the laboratory. Using these values the hydrogen ion concentration from the CO_2 contribution is evaluated to $(1.71^{+0.09}_{-0.10}) \cdot 10^{-6}$ M. If instead the equilibration temperature is assumed to be 45°C the CO_2 contribution is evaluated to $(2.18^{+0.11}_{-0.13}) \cdot 10^{-6}$ M, which is about half the hydrogen ion concentration actually measured on average.

5.1.2 Response times

In order to estimate the temporal resolution, the signal response time was investigated. The response time is the time it takes for the system to respond to a step function, which in practise is a change in standard solution, to increase from 5 % to 95 % of the change. Any signal shorter than this response time will not have full resolution. The response time was evaluated for all standard series run during the melting campaign for both phosphate and pH measure-

ment. However, in a standard series multiple standards were run right after each other, and the response time was evaluated for the magnitude of the change in concentration between standards, rather than the general levels in concentration, as proposed by [Rasmussen et al., 2005]. It was found, that in the linear range of phosphate, the response time for concentrations less than 0.4 ppb was 30 seconds while a change of 1.1 ppb had a response time of 59 seconds. The rise in response time with increased concentrations seems almost logarithmic, but the number of data points is too small to quantify this statement. A plot of the response time for PO_4^{3-}, with uncertainties obtained from the data, is sown in figure 26, while the data for pH is found in figure 27. Both is to be found in the appendix section: Response times. In the case of the pH measurements, the response time seemed (almost) independent of concentration change, for concentrations above 10 μM, with a value of 43 seconds. These numbers should be kept in mind if the data exhibit rapid fluctuations.

5.2 Baseline and contamination

Analysing the standard solutions is all about getting a reference point, or rather a calibration curve, that can be used to convert the light intensity into impurity concentrations for ice core samples. As stated by the Lambert-Beer law, this requires that one knows both the signal intensity of the transmitted and the incident light. The absorption associated with the incident intensity is known as the baseline signal, and this is what provides the link between the samples, and the standard solutions. The reason for this is that the general intensity of the light signal may change between standard runs, due to e.g. air bubbles or dust getting stuck in the flow cell, and the baseline is a measure of whether this is the case. Hence it is important to get a good estimate of the baseline values. During the melting campaign, the phosphate baseline ranged in value from ~14.000 to ~30.000, but it never changed by more than about 1000 counts on any given day. Due to a change in integration time for the pH signal, the intensity for pH ranged from ~7.400 to ~53.000, but again the relative change on any given day was much smaller.

Even though the change in intensity on any given day is small, significant changes may still occur during a run. If dust or air got stuck in the flow cell a rapid change in the intensity occurred, or more commonly if an air bubble moved through the cell changing the flow and hence the intensity slowly. An example of such a drift can be found in figure 14. To test whether or not any such significant changes had happened either during a standard run or during sample melting, a Student's t-test was performed on the distribution of intensities before and after the measurement in question. If this test failed on a 5% confidence level, adjustments to the data had to be made. If the change was caused by drift in the signal, a linear interpolation of the baseline before and after measurement was used, while sudden changes in baseline level had to be dealt with by analysing the section before and after the change separately, using the blank before and after as separate baselines.

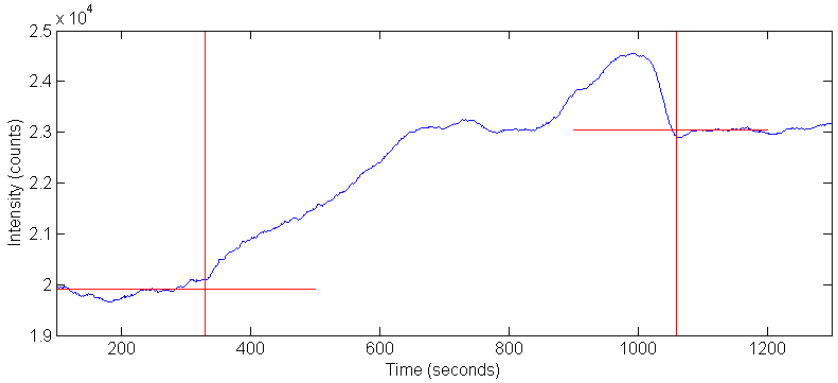

Figure 14: Example of baseline drift, here in the pH line. The red lines shows the level of baseline, and the onset and end of the standard run.

Unfortunately, in the case of phosphate, there was a need for further adjustments of the baseline during the melting campaign. This is due to an apparent phosphate contamination of the milli-Q water system, possibly caused by an old cartridge. It should be mentioned that these PO_4^{3-} contaminated milli-Q samples occurred at the same two days of measurement as the bad pH standards, and hence that these bad measurement might have a common cause, although phosphate and pH did seem to be the only detection lines affected by this contamination. Other explanations of the apparent phosphate contamination include changes in the reagent mixing temperature and flow changes due to valve changes in the system. Both were investigated and ruled out. Likewise a new accurel, a new dye mixture and new reagent and buffer was incorporated in the setup without removing the problem.

For the standard runs both the baseline and the different standard samples were based on the contaminated milli-Q water, but this should have little effect, due to all intensity measurements being shifted the same proportion. During melting however, this contamination was quite clearly visible. As the choice of detection technique for phosphate were based on absorption methods, any increase in the phosphate content of the sample should decrease the intensity of the transmitted light, just as is seen for the standard run in figure 10.

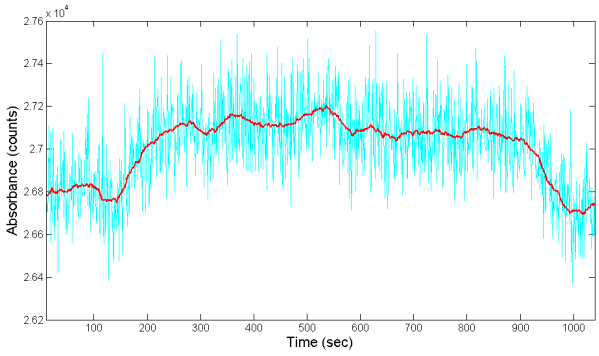

Figure 15: Example of an ice core sample, where the baseline has been affected by phosphate contamination of the milli-Q water. The blue curve is raw data, while the red is smoothed over 40 seconds. Data is from January 29, bag 58.

In the case of the contaminated milli-Q water, the response was quite different, as the intensity seemed to increase. An example of this can be found in figure 15. After the above mentioned attempts to better the response had failed, the most logical explanation was that the firn ice core samples simply contained less phosphate then the milli-Q water in the laboratory. The implication of this was that the baseline values could not fully be trusted in relation to the ice core samples. In order to proceed with the data analysis, it was decided to use the highest value of intensity from the sample as the baseline, as this corresponds to the least amount of phosphate, and is the closest to clear water the data could provide. This of course results in increased uncertainties in the baseline value, but allows for calculations of the general level and trends in phosphate concentration of the ice samples.

5.3 Errors and uncertainties

As mentioned in section 5.1.1, the error on the calibration curves were due to the uncertainty in the concentration of the standards used, as well as the noise on the intensity corresponding to those standards. With errors on both variables, a linear least squares approach was used to calculate the uncertainties on the slope, a, and the intercept, b of the calibration curve, as well as to find the standard deviation on these values. From equation (4.1) it is known that the concentration of a chemical impurity in the ice obtained by absorption methods, can be calculated as

$$c = \frac{\text{Abs} - a}{b} = \frac{-\log\left(\frac{I}{I_0}\right) - a}{b}, \tag{5.3}$$

and hence that, by error propagation, the standard deviation on the concentration is to be calculated by

$$\sigma^2_{[c]} = \left(\frac{\partial c}{\partial I}\right)^2 \sigma^2_I + \left(\frac{\partial c}{\partial I_0}\right)^2 \sigma^2_{I_0} + \left(\frac{\partial c}{\partial a}\right)^2 \sigma^2_a + \left(\frac{\partial c}{\partial b}\right)^2 \sigma^2_b \tag{5.4}$$

where σ_I and σ_{I_0} the uncertainty on the intensity of the transmitted light and the baseline respectively. They were assumed to be equal, and found by evaluating the standard deviation of the smoothed signal response to the milli-Q water baseline obtained before and after an ice core sample had been melted. In the case that the milli-Q water was contaminated with phosphate, the standard deviation was assumed to be double the standard deviation of the milli-Q baseline.

CHAPTER

6 Results and Discussion

In this section the results obtained from the 66 meters of the NEGIS shallow ice core processed with the CFA system of section 4.3 and the methods of chapter 5, is presented and discussed. Both the phosphate and the acidity detection proved successful in quantifying the content of impurities in the melt water, with the exception of the two days on which the standard solutions were affected by contaminated milli-Q water.

6.1 Results

Plots of concentration levels of the chemical impurities detected in the NEGIS shallow core can be found in figure 19 and 20. The average concentration of PO_4^{3-} was found to be 3.33 nM (0.32 ppb), with a standard deviation of 1.71 nM (0.16 ppb). Both numbers was obtained using the highest blank intensity response as the baseline, and a calibration curve using the three weakest standards of table 4. This configuration was found to be most plausible, but other configurations were calculated as well. Estimates of concentration levels and fluxes using other baseline values and calibration curves can be found in table 5. The maximum of detected phosphate was 12.60 nM (1.20 ppb), at a depth of 3.4 meters (2004 A.D.), although three instances of unusually large phosphate peaks were also detected at depths of 13.5 m, 42.6 m and 43,7 m (1967 A.D., 1793 A.D. and 1787 A.D.), and ranged to a maximum of 25.9 ppb, 4.42 ppb and 8.07 ppb respectively. These unusual response signals occurred at times when air had been detected in some part of the CFA system, and no correlation to changes in concentration of the other impurities could be found. Therefore these spikes might be associated with air bubbles as well. Correlations has been calculated for the dataset without these three peaks included, since based on Chauvenet's criterion these three peaks are to be considered as outliers caused by air bubbles, and hence excluded from the dataset.

The phosphate flux was calculated using equation (6.1), where ΔPO_4^{3-} is the mean phos-

phate concentration over one annual layer, acc is the accumulation rate and $\rho_{ice} = 917\,kg/m^3$ is the density of ice:

$$PO_{4,\,flux}^{3-}\left[\frac{\mu g}{m^2 yr}\right] = \Delta PO_4^{3-}\left[\frac{\mu g}{kg}\right] \cdot acc\left[\frac{m}{yr}\right] \cdot \rho_{ice}\left[\frac{kg}{m^3}\right]. \tag{6.1}$$

The accumulation rate is entered in ice equivalents, and can be calculated based on the annual layer thickness and density measurements performed on the NEGIS core. For the entire core this results in a mean value for the flux of $(24.2 \pm 11.9)\ \mu g \cdot m^{-2} \cdot yr^{-1}$. A plot of the evolution of the phosphate flux during most of the 18^{th} century, can be found in figure 17, and a histogram of the phosphate detected in the NEGIS core can be found in figure 16.

A spectral analysis was performed on two sections of the core. The annual layer thickness in this section was found to be 0.123 meters and 0.166 meters respectively for the two sections. The cut-off length found as five times the noise was between 1.14 and 1.44 cm. The spectral representation of the data can be found in figure 24.

Baseline:	**high baseline**	**high baseline fz**	**avg. baseline**
Unit:	ppb	ppb	ppb
Year 1900 – 2005 A.D.			
Mean	0.317	0.269	0.226
Std.	0.162	0.149	0.159
Var.	0.026	0.022	0.025
Year 1700 – 1800 A.D.			
Mean	0.295	0.224	0.237
Std.	0.116	0.115	0.111
Var.	0.013	0.013	0.012
Year 1995 – 2005 A.D.			
Mean	0.405	0.343	0.317
Std.	0.226	0.220	0.207
Var.	0.051	0.048	0.043

Table 5: Concentrations, standard deviations and variance of PO_4^{3-} in the NEGIS shallow core, found using three different calibration curves. The first column uses the largest intensity signal as the baseline value (high baseline), the second column uses the same approach, but the baseline is further assumed to be identical to a zero PO_4^{3-} concentration (forced zero). The last column uses an averaged milli-Q response as baseline. The data is for the period 1900 to 2005, 1700 to 1800 and 1995 to 2005 respectively.

6.2 Concentration levels and trends

Due to its remote location, not much is known about the concentration of phosphorus in the Arctic in general, and very few measurements of phosphate in ice cores has been carried out. Previous estimates has found levels of (0.32 ± 0.27) ppb for the most recent 120 years

measured in the shallow firn core NEEM S1, [Kjær et al., 2011], and Edwards et al. [2007] has found the mean phosphorus concentrations over the 20th century to be 0.25 ppb using ICP-MS, which measures the total phosphorus rather than the reactive part detected by the absorption method used in this thesis. Concentration levels at around these two values were therefore expected in the NEGIS shallow ice core as well. Edwards et al. [2007] furthermore found that the Phosphorus concentration had increased dramatically from 1990 to 2005.

The average level of PO_4^{3-} found in the NEGIS shallow ice core can be found in table 5, and the time series response in figure 19. It appears that the different approaches to choosing a baseline result in different estimates of the concentration level, which was to be expected. The first column in table 5, representing the baseline chosen as the highest intensity signal, is probably the one in which the most trust should be placed. This is due to the possibility of the milli-Q water being contaminated, in which case forcing the calibration curve through a zero point (column two) that is not actually known to be zero, will result in uncertainties of unknown magnitude. The contamination problem is believed to be localized to two days of measurement corresponding to the years 1835 to 1897, and hence the data in table 5 should not be affected by the contamination, but still the non forcing calibration curve is to be preferred. The average baseline (column three) might be artificially low due to any fluctuation in the response signal to milli-Q water, which will always tend to lower the baseline value. Common to all of the above values, is that the concentration levels are very low, and that within the uncertainty levels, the mean value of each approach cannot with much certainty be told apart. Figure 16 is a histogram of the phosphate detected in the NEGIS shallow ice core. It appears that a few instances of negative concentrations occurred, which is likely due to changes in baseline during measurement that has not been fully corrected for. From the histogram it would seem that the phosphate concentration is normally distributed, although the right tail is somewhat thicker than a pure Gaussian due to a number of spikes in PO_4^{3-} levels in recent times, see section 6.2.1.

The average concentration of phosphate found to be (0.32 ± 0.16) ppm for the most recent century is very close to the levels found by Edwards et al. [2007]; Kjær et al. [2011]. The NEEM S1 data was prepared using almost the same setup as was used for this thesis, so the results should be directly comparable, not least because both shallow cores analysed (NEEM S1 and NEGIS) was drilled roughly in the same part of Greenland, limiting any latitudal differences in phosphorus deposition. Both cores found the same average concentration of 0.32 ppb. Edwards et al. [2007] on the other hand measured using an ICP-MS technique, which detects total phosphorus. Since the reactive part of phosphorus/phosphate is only expected to be around 32 % of the total phosphorus level, [Mahowald et al., 2008], it was expected that the level found by Edwards et al. [2007] would have been higher than what was found in this thesis. Based on the 0.25 ppb of Edwards et al. [2007], a level of around 0.1 ppb was to be expected using DRP absorption methods. However, it should be noticed that the discrepancy is almost within one standard deviation of the 0.32 ppb found in this thesis. The discrepancy could also be an artefact of latitudinal differences and transportation patterns, as the ice samples Edwards et al. [2007] used for analysis were all located further to the south on

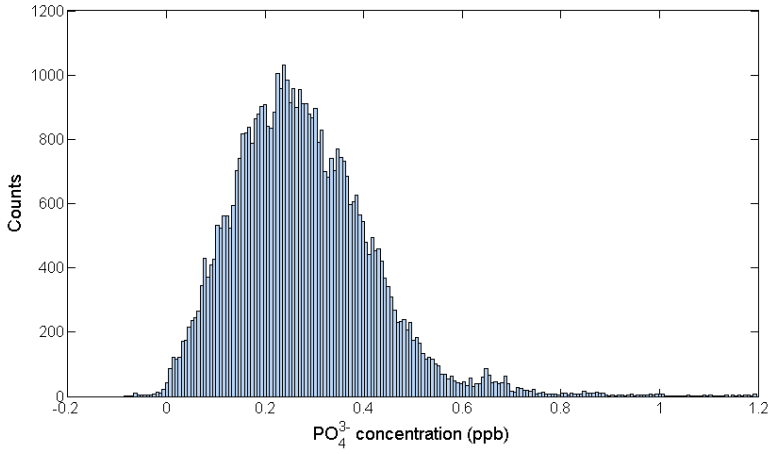

Figure 16: Histogram of the distribution of phosphate concentrations for the entire NEGIS shallow ice core. The high baseline non forcing approach was used to construct the histogram, and the data was smoothed over 40 seconds.

Greenland. Also if the amount of nonreactive phosphorus in the ice is low, the two results should be closer than what is expected from the 32 % ratio. Nenes et al. [2011] argues that this is indeed possible, as discussed in section 6.5.

The flux of phosphate together with the phosphate concentrations detected is presented in figure 17 for a subsection of the ice core spanning the time period 1720 to 1820. This period include several large volcanic eruptions, and was used to examine the effect of volcanic eruptions on PO_4^{3-} levels, section 6.5. The mean value of the flux in this period is $(26.9 \pm 11.1)\ \mu g \cdot m^{-2} \cdot yr^{-1}$, while the level for the whole core is $(24.2 \pm 11.9)\ \mu g \cdot m^{-2} \cdot yr^{-1}$. Apart from a few spikes in flux intensity the level seems to be almost constant. As a comparison, an earlier study of phosphate flux levels at the NEEM S1 drill site found a mean phosphate flux of 5.86 ng/cm^2/yr, [Kjær, 2010]. When the units have been converted, this turns out to be slightly more than double the flux, or almost three standard deviations above, the flux found in the NEGIS core. The difference might be caused by the NEGIS shallow drill site being located further inland as well as more to the east, than the NEEM S1 drill site, see figure 1. Given that the general wind direction on Greenland is from the west, it might be that more phosphate has simply been deposited en route, and the phosphate flux in central/east Greenland is smaller than for west Greenland. Since phosphate detection in in ice samples are a relatively new development, no other records were available for a comparison to investigate this hypothesis.

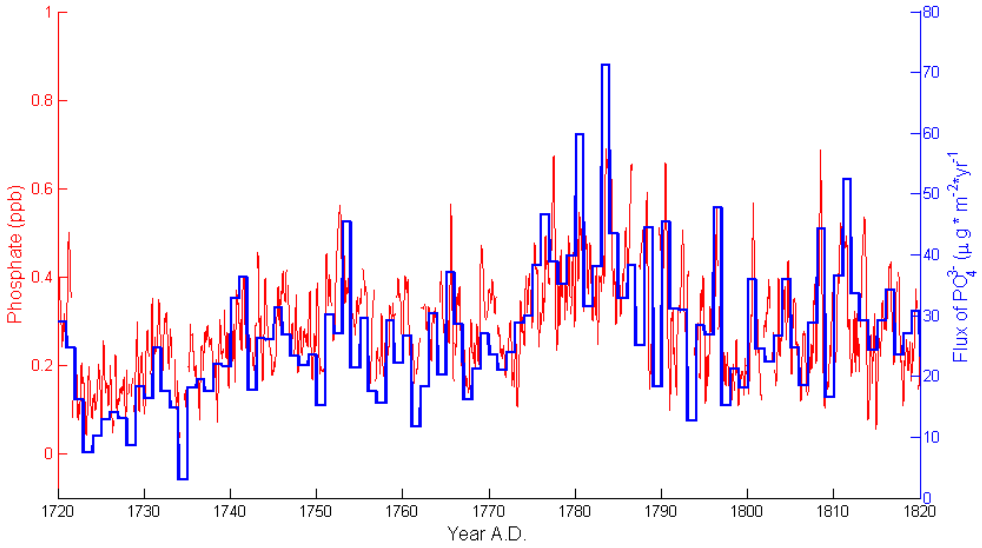

Figure 17: PO_4^{3-} flux and concentration level for the years 1720 to 1820, a time period including several large volcanic eruptions, e.g. Katla, Laki and Tambora. In red is the concentration level, and blue is the flux for the given year.

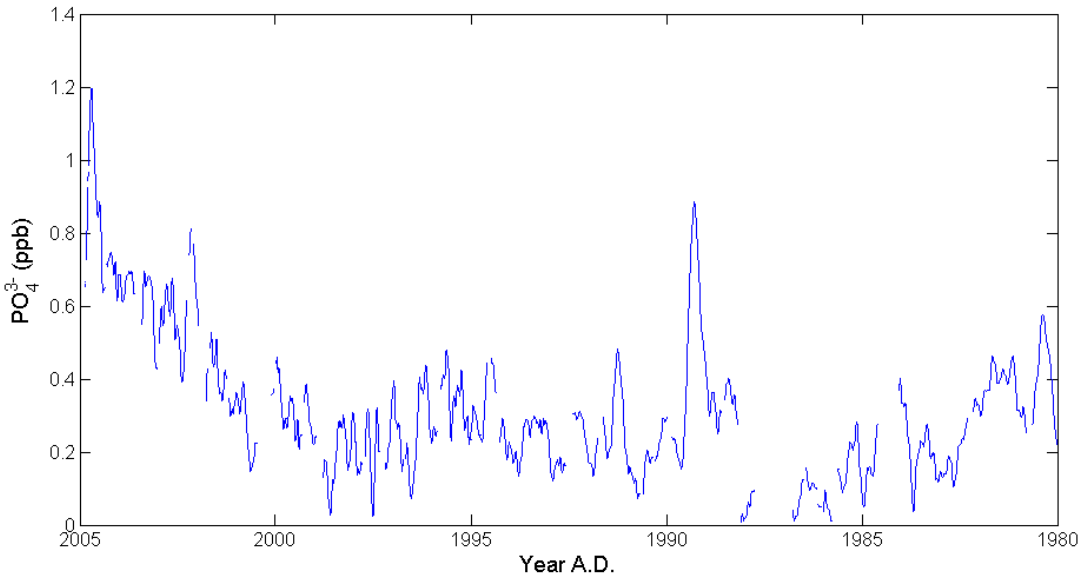

Figure 18: Phosphate concentrations for the period 1980 to 2005.

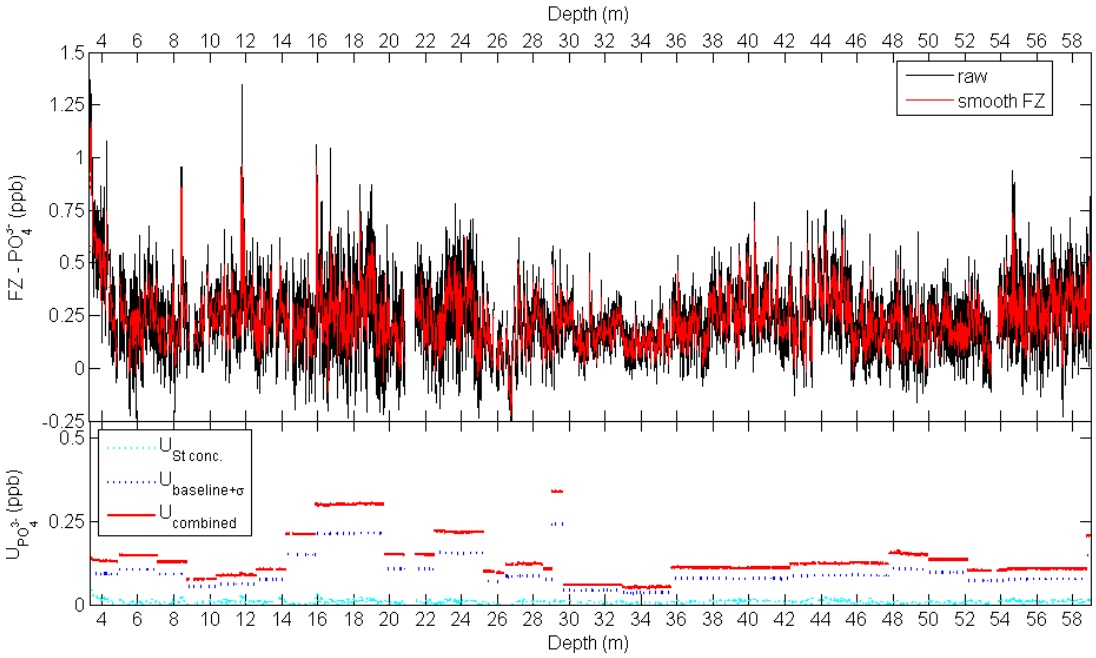

Figure 19: NEGIS PO_4^{3-} record of the entire shallow ice core. In the top is phosphate in raw (black) and smoothed (red) format, while the lower plot illustrates the uncertainty level. In cyan is the uncertainty on PO_4^{3-} caused by the uncertainty in the concentration of the standard solutions used. The blue curve illustrates the uncertainty from the choice of, and noise in, the baseline used, and the red curve is the combined uncertainty. A more detailed representation can be found in figures 20 and 21.

6.2.1 Anthropogenic phosphate

From the 400 years of data in the NEGIS shallow ice core, no trend was immediately visible for the PO_4^{3-} data, although some high spikes are present in the newer part of the ice. From the consumption of phosphate shown in figure 2, it could be expected that the steep rise in phosphate rock consumption during the later part of the 20th century would be present in the record, but this would seem not to be the case, as DRP levels in the NEGIS core remain stable over the entire core. According to Mahowald et al. [2008]; Smil [2002] as noted in section 2.1.1, human activities still only represents a small part of the phosphate global flux, with only about 14.3 % of the signal being anthropogenic. Given the accuracy of the NEGIS phosphate data, this would simply be too small an increase to be detected using the current system, due to the noise level (of around 0.17 ppb).

Even though no clear evidence of anthropogenic phosphorus was present in the NEGIS shallow core based on general trends in concentration, some indications of human activities may still be present. As mentioned, a number of phosphate spikes was detected, and the frequency of these events seems to have increased dramatically in the 20th century. Nine spikes larger than three standard deviations above the mean was detected at depths corresponding

to the years 1786, 1790, 1950, 1954, twice in 1975, 1989, 2002 and 2004, three of which can be found in figure 18. It has been speculated, [Mahowald et al., 2008; Pasteris et al., 2009], that due to more frequent occurrences of forest fires in recent times, the concentration level of phosphate should increase as well, but no clear correlation between phosphate and ammonium that normally signals biomass burning was found to explain the phosphate spikes.

Also Edwards et al. [2007] found that phosphorus increased dramatically from 1990 to 2005. From figure 18 it can readily appreciated that the same holds true for the NEGIS shallow ice core, but the concentration levels can also be found in table 5, and here it is clear that the increase is actually within the uncertainty. At best this can only be taken as an indication that human activities actually does have an impact on the phosphorus level, but also that there is no clear evidence of any anthropogenic changes.

6.3 Discussion of phosphate in the NEGIS shallow core

In this section the phosphate observations of the NEGIS shallow core is discussed in relation to dust, ammonium and sodium observations. The relation between the different chemical species in the core is investigated using correlations of the core as a whole, as well as running correlations to find any trends. The same smoothing was applied to all data series, since any rapid fluctuations caused by high resolution would ruin the correlation with a highly smoothed signal. 1 cm smoothing was used.

6.3.1 Dust

As shown by table 2, approximately 50 % of the phosphate should arrive directly with mineral dust on a global scale, which would suggest a large correlation between phosphate and dust. This estimate on correlation should be further increased if any phosphate sources have similar transportation patterns as dust. Even though the shape of the phosphate signal in many ways resemble that of the dust (see figure 20), it is quite obvious that the dependence is not linear. This can be explained if the dust contains different amounts of phosphate, or if as mentioned above additional sources of phosphate with similar transportation patterns exists, since this would constitute an underlying signal that could enhance the PO_4^{3-} signal whenever the signals coincide. It might also simply be that the transportation processes of dust and phosphate is similar in the way that PO_4^{3-} sticks to dust during transportation, but that the sources are different, or that the solubility of the total phosphorus in mineral dust varies. As mentioned previously, Mahowald et al. [2008] has found that the solubility fraction ranges between 7–100%.

To investigate whether dust particles is a source and/or a transport mechanism for DRP, the theoretical amount of PO_4^{3-} from dust sources can be determined and compared to the NEGIS record. To do this, it will be necessary to make some assumptions about the typi-

cal dust source for Greenland. According to Paytan and McLaughlin [2007], the P content of mineral dust is similar to the crustal abundance, which as mentioned in section 2.1.1 is between 700 and 1300 mg/kg. If we further assume that all the phosphate in dust is soluble, which might not be far from the truth (section 6.5), then the amount of dust borne P can be estimated by using the relationship $\log_{10}(\text{CCmassconcentration}) = (0.9084 \pm 0.0309) \cdot \log_{10}(\text{Abakus counts}) - (1.3276 \pm 0.1076)$, which approximates the number of dust particles found by the Abakus to the weight of the dust particles, [Kjær et al., 2012a]. Here the Abakus counts is in counts/mL and the mass concentration is in μg/kg.

Using this equation and a mean level of dust in the NEGIS core of 4085 particles/mL, one arrives at an estimate of 89.7 μg/kg, which with 1200 mg P/kg gives 3.5 nM P, which is very close to the 3.33 nM found by direct measurements. However, this was calculated using the assumption that all the phosphate in dust was dissolved, and even relatively rich in P. If this is not the case, the amount should be lower. Other estimates of the amount of soluble P to total P has been found to be 1-23 μg P/g soluble to 230-670 μg P/g total P, or about 0.2 % to 3.4 %, [Hodson et al., 2004]. In this case the amount of P from dust would more likely be around 0.1 nM. However, according to Nenes et al. [2011] this solubility fraction is much too low. Other estimates using dust counts from the GRIP ice core also suggests that dust is a major source of DRP in the NEGIS ice core, [Kjær et al., 2012a].

The calculation of correlation coefficients between elements in the ice core was done on several ways. First by simple correlation calculations, but to avoid any artefacts from changes in baseline of the different chemical components and see if the correlation was depth dependent, the correlation between species was also calculated in segments of 50 centimetres at a time (approximately five years depending on the depth), to produce a running correlation for the whole core. This further allows for uncertainty estimates on the correlation values. Using this approach the correlations between species was calculated to the values to be found in table 6, which is simply the averages of the running correlations. For dust/phosphate the running correlation value averaged 0.40 ± 0.21, and a standard correlation of 0.23 (including the corrupted parts of the ice). In doing the calculations it was further decided to leave out the data that had possibly been affected by the milli-Q contamination affecting the data from the later part of the 19^{th} century. This implied using the top or the lower part of the firn/ice core. The lower part from 35.8 meters to 59.0 meters, which spans a time period of 169 years, was used in the following. In this sense the correlation values only mirror the lower part of the core, where some amount of diffusions may have occurred. It is thus possible that the correlation values might be a little higher in the uppermost part of the ice sheet. Example plots of the running correlation coefficients can be found in figure 28 and 29 in the appendix. In these plots both the running correlation using intervals of 50 centimetres and of 1.0 meter respectively are shown, in order to estimate the impact that different interval lengths have on the estimated value. The two curves is in good agreement, but naturally the smaller intervals show more detail and variation.

From table 6 it would appear that phosphate is well correlated to dust, but on a closer look the tabulated number might not tell the whole story. By looking at the evolution of the phos-

	PO_4^{3-}	Dust	Cond	Na	NH_4^+
PO_4^{3-}	1	0.40 ± 0.21	0.49 ± 0.20	0.17 ± 0.28	0.11 ± 0.26
Dust	0.40 ± 0.21	1	0.31 ± 0.21	0.26 ± 0.29	-0.08 ± 0.19
Cond	0.49 ± 0.20	0.31 ± 0.21	1	0.26 ± 0.23	0.15 ± 0.23
Na	0.17 ± 0.28	0.26 ± 0.29	0.26 ± 0.23	1	-0.27 ± 0.18
NH_4^+	0.11 ± 0.26	-0.08 ± 0.19	0.15 ± 0.23	-0.27 ± 0.18	1

Table 6: Correlation coefficients for the chemical species in the NEGIS shallow core, as calculated by averaging the running correlations. In all instances the uncertainty on the correlation coefficient is in the range 0.18 to 0.29 found as the standard deviation of the running correlation, and is hence of comparable magnitude to the coefficients themselves.

phate to dust correlation, figure 28 in the appendix, it would seem that the correlation gets lower as the depth increase. This may indicate that phosphate is prone to diffusion in the firn layer. However, even in the deeper parts of the core there still is strong correlation, especially when one is only looking at extreme events. Figure 20 shows data for all measured species (except pH) for the period 1770 – 1820 (38.4 m – 46.2 m). In this section of the core eight dust spikes ranging more than three standard deviations (σ = 3919 mL^{-1}) above the mean (μ = 4086 mL^{-1}) occurs, and all of these peaks is matched by elevated levels in PO_4^{3-} concentration as well. This suggests that dust indeed is a strong source of DRP, although spikes in PO_4^{3-} that is not represented in the dust signal also occurs. The later is more pronounced in the upper part of the firn core. In figure 21 the data for the time period 1950 – 2005 is shown. Here seven spikes of excessive DRP occurs (more than three standard deviations above the mean), only one of which seems to be correlated with dust. This indicates that other sources than dust is needed to explain the DRP levels in full, especially for the younger ice. Some of the answer may be found in correlation with ammonium.

6.3.2 Ammonium

The correlation between ammonium and phosphate is in general very low, table 6 and a normal correlation value for the entire core of 0.03, but as mentioned in section 2.1.1 it has been speculated that the origin of some of the high spikes in DRP might have been caused by forest fires in North America (due to general wind directions towards Greenland). It has been speculated that spikes in NH_4^+ in ice records can be associated with the burning of biomass, [Fuhrer et al., 1996], but in the case of the NEGIS firn core none of the extreme spikes in DRP coincide with extreme spikes of NH_4^+, with the sole exception of the occurrence of the Laki volcanic eruption. Even the largest spike in NH_4^+ ranging more than 14 standard deviations above the average could not be associated with any increase in DRP.

Even though there is no correlation between NH_4^+ and PO_4^{3-}, the original paper by Fuhrer et al. [1996] also found no correlation between the NH_4^+ concentration, and the area of forest that had burned in North America. It was therefore assumed that NH_4^+ is simply not a good

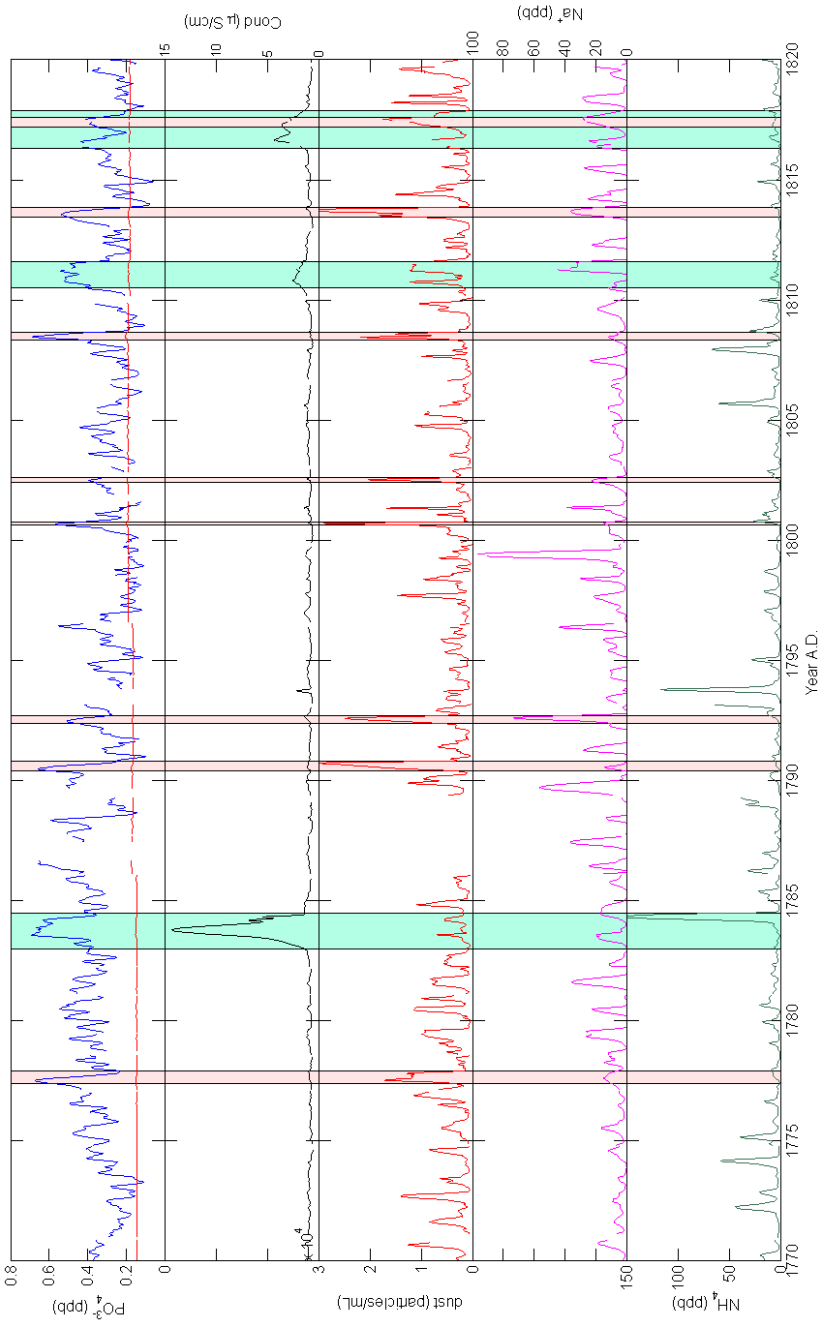

Figure 20: In the top is the DRP concentrations on an age scale with 1 cm smoothing, as detected in the NEGIS shallow ice core (blue) together with the combined uncertainty budget for DRP (red). Beneath is conductivity, dust, sodium and ammonium, all with 1 cm smoothing. The blue bands represent volcanic eruptions, with Laki (1783), an unknown volcano (1810) and Tambora (1816) represented. The red bands indicate peaks of dust exceeding three standard deviations above the mean. The time period represented is the years 1770 to 1820.

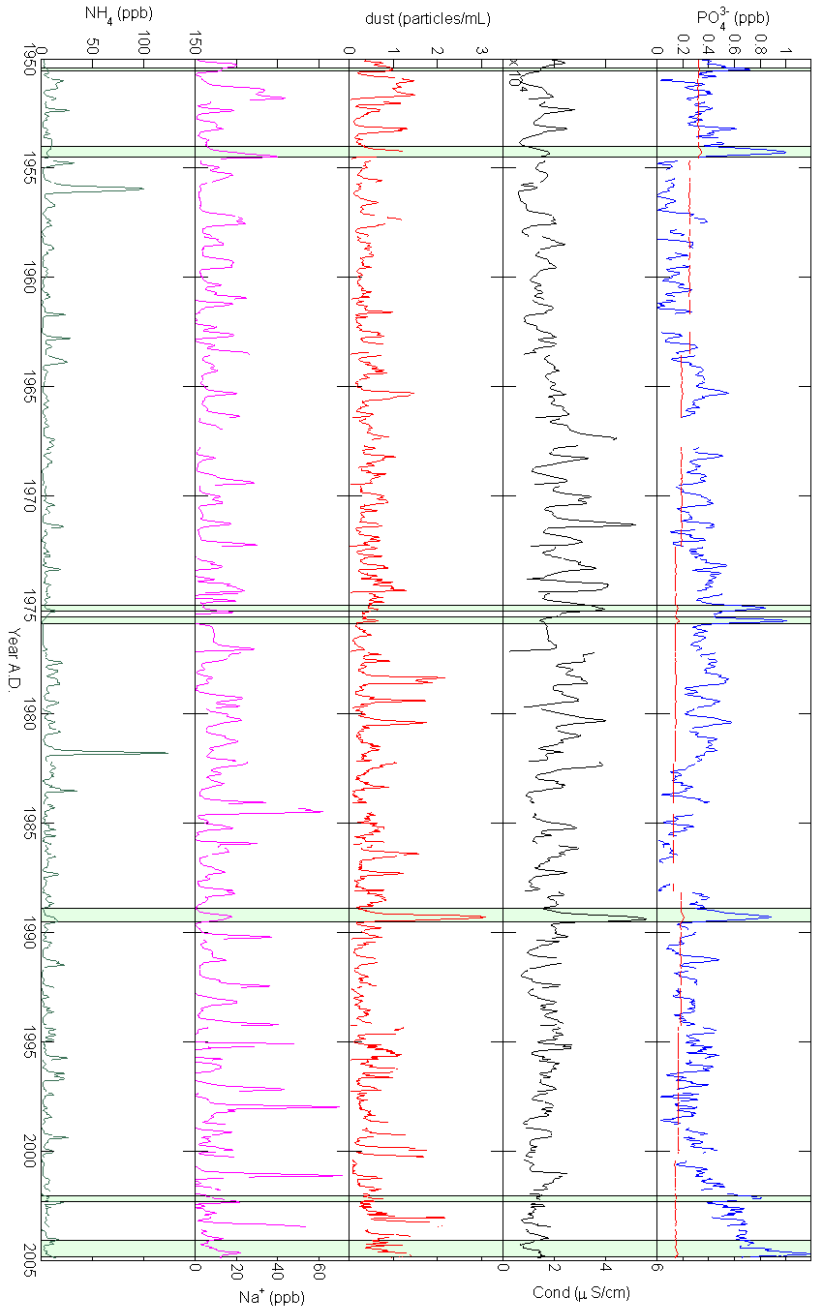

Figure 21: As in figure 20: In the top is the DRP concentrations on an age scale with 1 cm smoothing, as detected in the NEGIS shallow ice core (blue) together with the combined uncertainty budget for DRP (red). Beneath is conductivity, dust, sodium and ammonium, all with 1 cm smoothing. The green bars indicate peaks of PO_4^{3-} exceeding three standard deviations above the mean. The time period represented is the years 1950 to 2005.

proxy for wildfires, but that P might be. Since records of forest fires and their magnitude has only been kept extensively since the later half of the 19th century, only the part of the NEGIS core corresponding to the years 1950 – 2005 was compared to records of forest fires. Seven of the nine peaks in DRP reaching more than three standard deviations above the mean was found after 1950, se figure 21, where good records were kept, and hence these peaks was compared to a list of major wildfires in North America found at [Wikipedia, 2013a,b]. Of these seven peaks, the 1950, 2002 and the 2004 peaks were represented on the wildfire list. Two of these fires were the 1950 Chinchaga fire, supposedly the largest North American wildfire on record, and the 2004 Taylor Complex Fire, which is the largest wildfire by acreage of the 1997 – 2007 time period. Also one of the seven phosphate peaks correlated to the dust signal, as mentioned earlier. This suggest that the DRP spikes may to some extent be correlated to the occurrence of wildfires, even though these wildfires did not show in the NH_4^+ record, and only the largest fires were clearly represented. But the statistics on which this possible correlation is build is very limited, and therefore the correlation cannot be established with any certainty based on the NEGIS shallow core data. The relation could be investigated by measuring other tracers of biomass burning, such as vanillic acid, [Paterson and Cuffey, 2010], non-sea-salt sulphur, [McConnell et al., 2007] and K [Mahowald et al., 2008] but these are currently unavailable for the NEGIS core.

6.3.3 Sea salt

Like dust particles, sea salt has a small constituent that consist of phosphate, and like in the case of dust that means that a correlation was expected between sodium and DRP. However, while dust contains about 1200 ppm phosphate, the average concentration of phosphate in the ocean is only 0.088 ppm as compared to 10752 ppm Na^+ [Turekian, 1968], while Mahowald et al. [2008] estimated concentrations of 0.05–3.5 μM, and the amount of phosphate arriving with marine sources is usually very small. If one assumes that the ratio between the two elements on sea water is the same as the ratio in sea salt aerosols, then the ratio between the two elements and the level of Na^+ detected in the NEGIS core, can be used to evaluate the potential amount of phosphate arriving with sea salt sources, $ssPO_4^{3-}$. The average Na^+ concentration of the entire NEGIS core was (10.1 ± 11.3) ppb, giving a $ssPO_4^{3-}$ concentration of less than 0.003 nM P, as compared to the average 3.33 nM P of total DRP actually detected. Furthermore, no obvious match between spikes in DRP and Na^+ occurs, and the running correlation of (0.17 ± 0.28) (standard correlation of 0.03) is also far from enough to establish a relation between the two elements. A sea salt source for the DRP detected in the NEGIS firn core thus seems quite neglectable.

6.3.4 Seasonality of the phosphate signal

Based on the correlation values of table 6 and the clear indication of annual cycles found by spectral analysis, see section 6.6, it would appear that the deposition of phosphate displays seasonal variations. Being most strongly correlated to dust, the majority of the phosphate arrives in the boreal spring, while neither sodium (winter signal) nor ammonium (summer

signal) is correlated to phosphate within the uncertainty on the running correlation. As explained in the previous sections, dust is also the only source measured during the NEGIS melting campaign for which it was possible to find certain matches in elevation of concentration levels between species.

The high correlation to conductivity might be due to the solubility of phosphate being affected by acidic solutions, see section 6.5.

6.4 Conductivity, ECM, DEP and pH

As mentioned in section 4.4, the relation between the liquid electrolytic conductivity, the ECM and the DEP measurements are not straightforward, as many factors seem to influence the result of a measurement. In this section some of these issues are examined in relation to the NEGIS core.

The ECM data has been transformed to H^+ μeq L^{-1} by use of equation (4.5). The parameter values used are $c_1 = 0$, $c_2 = 4.5$ and $c_3 = 3$. c_1 can be used to allow the ECM to give a negative acidity, but according to Moore et al. [1994] positive values of the parameter can give problems in interpretation of low ECM values. Although due to uncertainties in the direct H^+ measurements, as well as the non-standard correction for density variations, the scale does not match up exactly with that found by pH measurements. The general level is about the same though, and trends in conductivity can still be compared. The DEP data was corrected for density variations as well, but unlike ECM the correction was only linear. Both the original ECM and DEP measurements as well as the density corrected versions, can be found along with liquid conductivity and pH in figure 22 for the whole NEGIS core, while a subsection spanning the first 50 years (1607 – 1657) can be found in figure 23. The major volcanic eruption signals have been marked, and can be found in table 7 as well. Notice that the section of pH data corresponding to approximately 1835 – 1897 shows somewhat larger variability than the rest of the core. This is due to the strange pH standard solution response, mentioned in section 5.1.1.

The relationship between ECM and DEP measurements has been treated quite extensively in the literature, and it is commonly agreed that both ECM and, if the salt content is known, DEP are excellent measures of acidity, [Hammer, 1980; Moore et al., 1989, 1992], although ECM is unable to measure the acidity of alkaline ice, [Moore et al., 1994]. Also agreed upon is that three chemical species (acidity, ammonium salts and most likely chloride) is enough to account for all peaks in conductivity, [Barnes et al., 2002; Moore et al., 1994]. Specific for ECM, is that it is only sensitive to H^+ concentration, while DEP is also sensitive to the salt content, [Moore et al., 1992, 1994]. The intensity of the ECM response seems to depend on the acidic species, e.g. H_2SO_4, HCl and HNO_3, causing the peak, [Wolff, 2000], which may complicate the interpretation somewhat if the salt content is not accurately determined. Finally large amounts of ammonium caused by biomass burning events or biogenic emissions usually has the effect of decreasing the ECM response rather than to increase it, [Moore et al.,

1994; Wolff, 2000], although this is explained by the weak acids, formate and acetate, that accompany these events associating with the acidity and making it unavailable for conductivity measurements, rather than as a direct response to the ammonium signal. Most of these papers however focus on ice cores rather than firn, [Barnes et al., 2002; Moore et al., 1994].

When looking at the data obtained from the NEGIS firn core, the main feature of figure 22, is that all the different conductivity measurements show some major common trends. All show a clear increase in acidity during the later half of the 20^{th} century, which was expected and corresponds to the substantial increase of SO_2 production by industrial activities, most significantly coal burning, [Paterson and Cuffey, 2010]. As mentioned in section 3.4, this SO_2 is transformed to SO_4^{2-} and sulphuric acid by atmospheric oxidation. Also, all four measurements show a slow decrease in these industrial levels of sulphuric acid, after the Clean Air Acts of 1970, 1977 and 1990 had been implemented. The last major trend found in the NEGIS firn core measurements is the volcanic spikes, although not all of them can be seen quite clearly, or to the same extend using different detection techniques.

Notice that the large amount of air in the upper part of the firn core is sufficient to almost hide the industrial rise in sulphuric acid in the ECM and DEP signal, and that these can again be brought out by the crude density corrections applied. This indicates that density correction most likely should be applied in close to the way that it was done, even though the parameters of the fit might not be exact. pH and liquid conductivity are of course measured on melt water, and hence they are not susceptible to density changes.

When calculating the correlation between acidity and liquid conductivity, it appears that the two are almost identical in evolution. If the section of the ice core affected by milli-Q contamination is ignored, one obtains a correlation of 0.80 ± 0.15 for the NEGIS firn core. Based on this correlation, measuring acidity directly almost seems redundant, given the accuracy and ease of liquid conductivity measurements. However, even though the correlation at NEGIS is very good, it may not be in general. The conductivity is governed by all the ions in the melt water, while the acidity is determined almost exclusively by the H^+ content, although neglectable amounts of Lewis acids such as Fe^{2+} or Mg^{2+} might be present. This means that for ice cores with more impurities such as the sodium rich cores from coastal Antarctica, [Moore et al., 1989; Wolff, 2000], the liquid conductivity and the acidity might not be so well correlated. For the relatively clean ice from the central part of ice sheets the differences are slight, but for a few important exceptions. The ECM signal is, like pH, supposed to account for H^+, so any differences between the two signals can be quite interesting.

From figure 23 it would appear that the two signals are anticorrelated once in a while, when the firn gets alkaline. This is most pronounced in the year 1617, with 1621 showing much the same features. When compared to the other chemical species detected, it turns out that these two years coincide with the largest and the third largest ammonium peak observed in all the NEGIS firn core. These two major peaks seems to confirm that ammonium, or at least its accompanying acids are able to lower the acidity, even to the point of it being negative. Since no large fluxes of dust were seen to account for the alkaline ice, the signal should

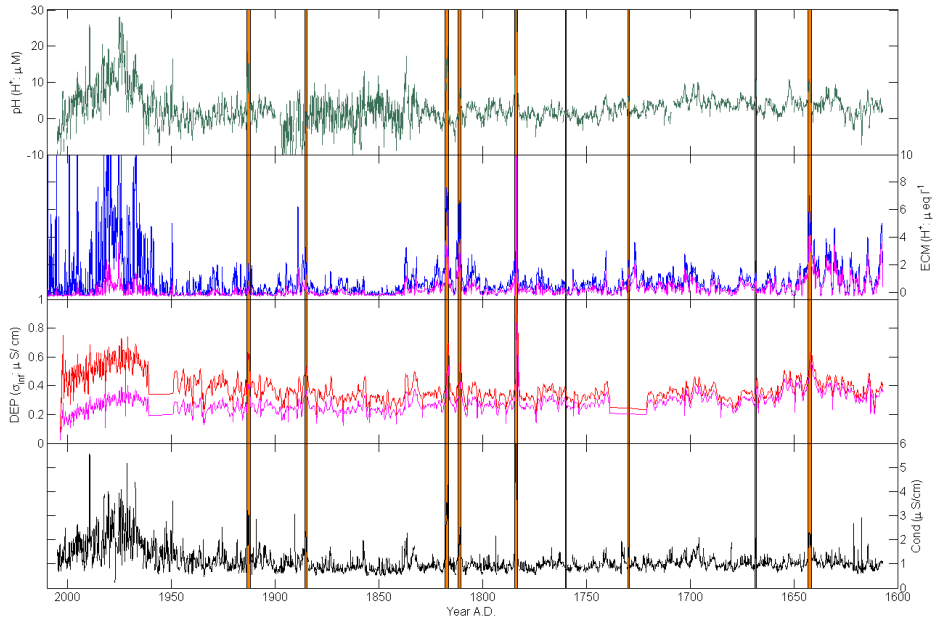

Figure 22: Comparison of the different conductivity measurements. From top to bottom the measurements are pH (green), ECM original data (magenta) and density corrected (blue), DEP original (magenta) and density corrected (red) and liquid electrolytic conductivity (black). Major volcanic eruptions has been mark by coloured bands. Only pH and liquid conductivity was measured during the melting campaign, while ECM and DEP had been measured previously.

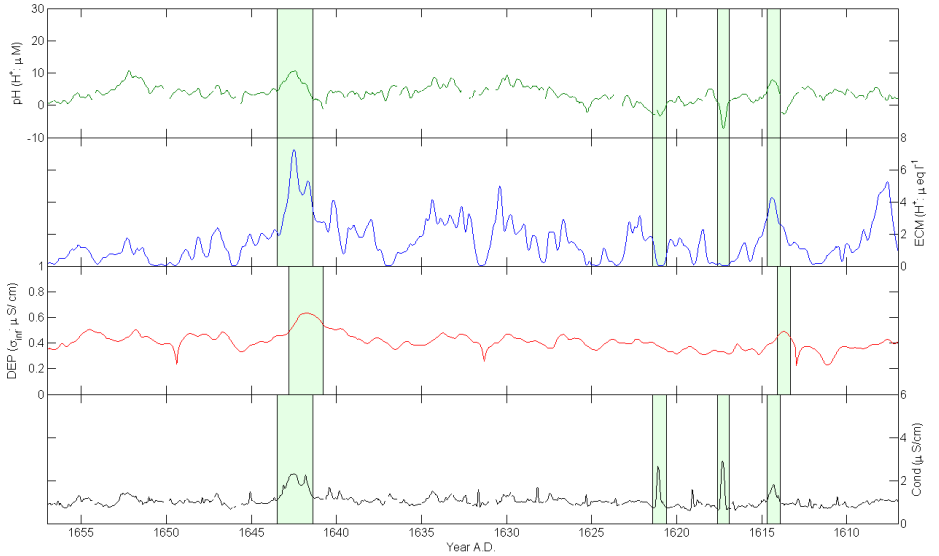

Figure 23: The measurements shown are the same as for figure 22, but constrained to the first 50 years of the data series, 1607 – 1657. The coloured bands indicate some of the similar features in the response signals. The DEP seems to be a little off, which should be kept in mind for comparison.

be caused by NH_4^+. As it turned out, this assumption was further strengthened by most of the ammonium peaks of more than three standard deviation above the mean, approximately 40 ppb, could be found as dips in the pH signal in all the NEGIS core as well. Since ammonium might be correlated with forest fires, forest fires might also be anti-correlated with the pH. These dips in acidity is also quite clear in the ECM data, which drops to zero as the acidity gets negative. The DEP on the other hand shows no response, which may be due to a larger smoothing inherent in the DEP measurement performed than what was applied to the other channels. In general though, the observations is in good agreement with the literature, but given the ad hoc density corrections and therefore quite uncertain acidity levels predicted by ECM and DEP it was not possible to calculate trustworthy correlation values, and thereby quantify the interrelationship of the different acidity channels. The density likewise makes it very difficult to constrain the major ion balance of the NEGIS firn core, as the absolute acidity levels based on the ECM and DEP data is not known.

6.5 Special layers

A few layers in the NEGIS firn core are of special interest, as they are expected to deviate from the norm. They are the volcanic layers, as well as the melt layer of 1889. Also some very strong signals in ammonium was addressed in section 6.4.

Melt layer: The melt layer should be of special interest as percolation should have penetrated the firn from the winter of the previous year, creating a smoothing effect and possibly changing the chemistry. The percolation could cause the impurities of a given year to be concentrated within the melt layer, [Alley and Anandakrishnan, 1995]. This effect was only seen very weakly in the NEGIS firn core, and unfortunately both the PO_4^{3-} and the pH line was affected by contaminated milli-Q water and bad calibration curves on the day the melt layer was reached, and nothing conclusive could be seen from these lines. However, of the other detection lines only the ECM line had any clear increase on signal, and the effect from the melt layer was most likely very limited.

Volcanos: A list of some of the major volcanic eruptions can be found in table 7. Most of the volcanoes listed in the table are visible in all the conductive channels, however eruption before Laki in 1783 are very weak at best. The increase in acidity is clearly seen as would be expected, but more interestingly, there seems to be a response in the PO_4^{3-} channel as well. This can be seen in figure 17 and 20, in which the Laki eruption are represented. Laki also provides one of the most convincing correlations between volcanic eruptions and increased levels of phosphate, although the effect can also be seen in some of the more recent eruptions. The average PO_4^{3-} concentration for the period 1720 – 1820 shown in figure 17 is (0.29 ± 0.11) ppb. During the eruption however, the concentration reaches a maximum of (0.80 ± 0.08) ppb, more than four standard deviations (4.43 to be exact) above the mean. Likewise the levels of the phosphate flux can be found in the same period, and it turns out that

the flux during the eruption is almost four standard deviations (3.72) above the average. This apparent increase in phosphate levels caused by volcanoes can be explained in several ways. It could be that the volcanic dust and gasses released into the air is simply rich in phosphate as compared to normal atmospheric aerosols. It could also be that the increased amounts of phosphorus is simply due to increased amounts of dust, but this seems unlikely based on the observations of the NEGIS core since not much dust is present during eruption. As a third option it might be that the P flux is actually the same whether there has been a volcanic eruption or not, but that the increased acidity following the eruption alters the solubility of phosphate and makes it reactive. This third option seems the most likely based on the NEGIS record, as a strong correlation between electrolytical conductivity and dust, (0.49 ± 0.20) as well as between phosphate and acidity (0.51 ± 0.23), were found. This correlation naturally centres around the SO_2 and NO_x background level rather than the rare volcanic eruptions, but still seems to show a relationship between acidity and phosphate solubility.

Volcano	**year**	**NEGIS depth [m]**
Katmai	1912	22.7
Krakatoa	1885	27.3
Tambora	1816	39
Unknown	1810	40
Laki	1783	44.3
Katla	1760	46.6
Lanzarote	1730	50
Pacay	1670	59
Komagatake	1640	62

Table 7: List of volcanic reference points that could be seen in the NEGIS shallow ice core from the DEP data.

The subject of soluble phosphate in airborne dust particles, and the change of solubility with acidity, has been treated by Mahowald et al. [2008, 2005]; Nenes et al. [2011], who also based their measurements on a molybdenum blue method. This choice should make the results directly comparable to the NEGIS results, although the area examined by Nenes et al. [2011] was the eastern Mediterranean. They found that the solubility of P from apatite dust is generally very variable, with soluble P varying between 3–10% of total P in Saharan dust. What is interesting is, that when exposed to a the humid and slightly acidic conditions due to pollution in the Mediterranean, the solubility increased by as much as 10–40 times, and in the case of Saharan soil and dust, 81–96% of the total inorganic P was released to solution following the atmospheric acid treatment. This result seems to agree with the NEGIS data, although it was not possible to assess the possible change in solubility in Greenland dust due to acidity, since this would require a detailed analysis of the composition of the dust in itself. Also the extent to which the NEGIS results can be directly compared to the findings of solubility under Mediterranean conditions might be limited, since some of the reason for

the high solubility of P found by Nenes et al. [2011] is caused by the high relative humidity of 80–95%. This allows for an aerosol solution of acid, water and dust that provide the medium for reacting and dissolving mineral-bound P. Since the Arctic atmosphere is generally much drier than this, it is unknown whether the same effect could take place there. No study was found that examined to solubility of P under Arctic conditions.

6.6 Spectral analysis

In order to evaluate the results presented in this chapter, several assumptions made regarding the resolution and periodicity of the chemical impurity signal needs to be reviewed in relation to the results obtained. It has been assumed that the resolution was sufficient to resolve annual layers, as well as that the resolution, or smoothing, on the data for different impurities is comparable. Whether this was actually the case, can be tested by analysing the power density spectrum.

Two subsections of the NEGIS firn core was subject to spectral analysis by fast Fourier transform (FFT) in order to investigate the resolution. Since the NEGIS core is a firn core, the annual layer thickness, based on layer counting of impurities, is quite variable, see figure 9. If the whole core was subjected to spectral analysis, a poor estimate from layer thickness would ensue. However, the layer thickness seems to be almost stable at depths between about 22 m and 46 m where $\lambda = (0.166 \pm 0.032)$ meters, as well as from about 48 meters to 66 meters, where $\lambda = (0.123 \pm 0.021)$ meters. It was decided to use both of these subsections of the NEGIS data for spectral analysis, since the first subsection spanned the 19^{th} century, the later part of which had been affected by contaminated milli-Q samples in both the pH and PO_4^{3-} line. It was expected that the contamination did not affect the behaviour of the concentration, but only the absolute values and the reliability of the fit parameters, and hence that it would still be a meaningful comparison. The upper subsection covered 146 annual cycles, while the lower section covered 140 annual cycles, and the minimum/maximum layer thickness was found to be 0.092/0.250 meters (upper section) and 0.078/0.187 meters (lower section) respectively, why the FFT was performed on a time scale.

As it turned out, both sections showed clear annual cycles in phosphate as well as for all other impurities. Figure 24 (B) and (C) shows the power spectra of the impurity record for sodium and phosphate in the time domain after applying the time scale resulting from the layer counting. In this domain spectral peaks corresponding to the annual cycle are quite significant for the samples. For the older section of the core the annual spectral peaks was only just visible, while it was much more pronounced in the upper subsection. This trend may be caused by diffusion. The periodicity is a strong indicator of visible annual cycles in the PO_4^{3-} data.

From the power density spectra in figure 24 (C) it is further clear that finding a good cut-off value is not easy. The spectrum seems to show a memory effect in the sense that a stable level of noise is not reached. As already mentioned, phosphate have a tendency to stick to

surfaces due to its overall charge, and this coating induces concentration dependant noise levels. However, it is still possible to give estimates of the cut-off value and hence the resolution. The resolution, based on the power spectrum, was found to be between 1.14 cm (5 standard deviations above noise), and 1.44 cm chosen by eye, and the cut-off showed almost no variation with depth. Both of these values are well below the annual layer thickness, and hence the setup should be capable resolving annual variations. These cut-off values are shown in figure 24 as vertical blue lines. These cut-off values correspond very nearly to the 1 cm resolution data used in the analysis, as well as the resolution set by the 30 seconds response time found in section 5.1.2. Any further decrease in resolution could be caused by capillary effect sucking water into the firn due to low flow rates as well as due to the memory effect of phosphate.

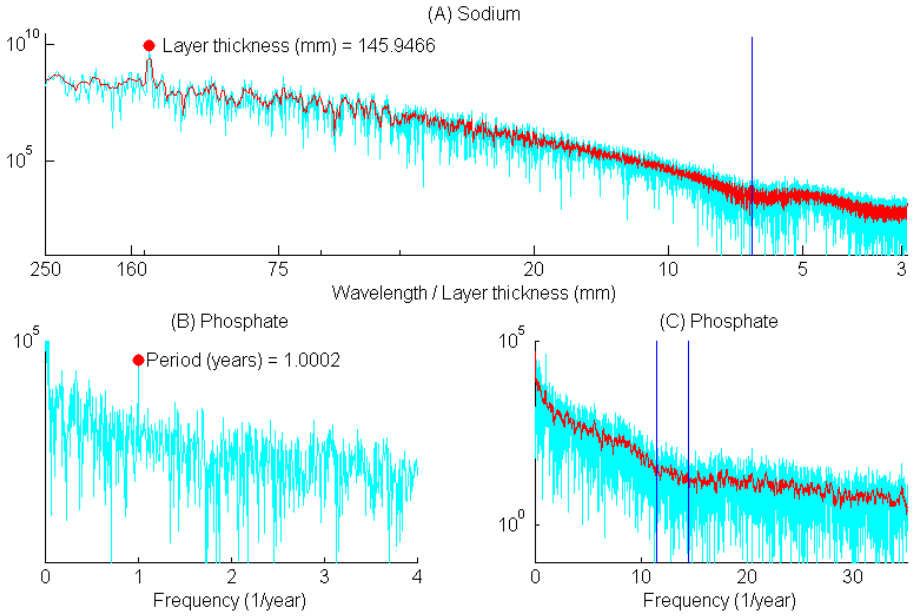

Figure 24: Power density spectra for PO_4^{3-} and Na^+. The top figure (A) is the depth domain density spectrum for Na^+, while the lower two show the time domain density spectrum for PO_4^{3-} in different degrees of detail, (B) is simply a close up of the low frequency part of (C). The spectra are obtained by FFT of 24.2 meter records in 1 cm depth resolution. Missing sample sections were skipped. Raw FFT response is shown in cyan, while a smoothed version is shown in red. The blue bars are cut-off values, bellow which the noise dominates the signal. Usually this cut-off is chosen as five times the noise, but is also associated with the kink in the curve when noise starts to dominate. This leaves room for a subjective choice of cut-off values.

CHAPTER

7 Conclusions and Outlook

In this study the first high-resolution continuous dissolved reactive phosphorus (DRP) and pH records from a Greenland shallow firn/ice core was presented. The detection methods used were the 2 m liquid waveguide capillary cell (LWCC) molydenum blue method developed by Kjær [2010] for the detection of DRP, while pH was measured with a spectrophotometric method adapted from Raghuraman et al. [2006], using a combination of dyes to measure acidity by absorption. These methods were successfully applied to a 66 meter shallow firn/ice core from the North East Greenland Ice Stream (NEGIS, 75.623°N, 35.96°W).

In the case of phosphate the data was divided into three sections, covering the preindustrial (1700–1800), the last century (1900–2005) as well as he most recent period (1995–2005). All showed similar concentration levels of DRP with 0.30 ± 0.12 ppb (3.1 ± 1.2 nM), 0.32 ± 0.16 ppb (3.33 ± 1.7 nM) and 0.41 ± 0.23 ppb (4.3 ± 2.4 nM) respectively, and all of these was within one standard deviation of each other. Thus no anthropogenic impact on DRP concentrations was observed, as compared to the preindustrial background concentration levels. However, in very recent times a general increase in concentration levels, as well as in the frequency of very large DRP peaks, above three standard deviations, seems to agree with the measurements of Edwards et al. [2007], although this could not be fully established within the uncertainty. The uncertainty on the measurements, resulting from baseline variability, standard reproducibility and calibration uncertainties were usually found to be bellow 0.2 ppb with an average of 0.17 ppb for the section of the core corresponding to the years 1770 – 1820. On two out of the twelve days in the measuring campaign, the phosphate and pH line was disturbed by contaminated milli-Q water standards, and for these measurements, much higher uncertainties of about 0.42 ppb phosphate were observed, rendering this data almost useless.

Subannual variations in DRP concentration levels were observed as well as clear seasonal cycles. The seasonal cycles did however seem to be affected by diffusion, as the signal got less pronounced with increasing depths. From correlation calculations it was found that DRP associates most strongly to dust, and hence that phosphate is a spring signal, while weak corre-

lations with sodium and ammonium indicates low phosphate concentrations in winter and summer time. Based on the amount of dust in the melt water, it was also found that mineral dust was enough to account for the main concentration levels, with biosperic emissions needed to explain some large spikes. Even though no correlation to ammonium was found, often strong DRP peaks could be found in years with large forest fires in North America, which might make phosphate an indicator of forest fires, but measurements of, and correlation to, other indicators of biomass burning needs to be undertaken to verify this.

A strong correlation between acidity and phosphate was also found, which seems to suggest that increased levels of acidic elements can change the solubility of inorganic phosphate in dust particles, and make it reactive. This hypothesis is also supported by a clear increase in both flux and concentration levels when volcanic eruptions occur.

Besides analyzing the phosphate, the acidity, electrolytic conductivity, electric conductivity measurements (ECM) and dielectric profiling (DEP) of the NEGIS core was completed and compared. The sample was heated to 65°C to equilibrate with the CO_2 concentrations in the laboratory, in order to account for the carbonic acid contribution to acidity. It was found that the CO_2 contribution could be responsible for as much as half of the average hydrogen ion concentration. The uncertainty on the partial CO_2 pressure in the laboratory had a range of about $0.2 \cdot 10^{-6}$ M. The temperature dependant equilibration time is believed to be well constrained, but this assumption was not validated. A decrease in temperature from 65°C to 45°C also increased the CO_2 contribution with $0.47 \cdot 10^{-6}$ M, which is about 15% of the average hydrogen ion concentration measured for most of the NEGIS core. For future use of the system it would therefore be recommended to adopt an approach similar to that of Pasteris et al. [2012], where the sample is equilibrated with a known partial pressure of CO_2, and is known to have had plenty of time to equilibrate.

Due to the NEGIS core being a firn/ice core, it was necessary to make rough density corrections of the ECM and DEP measurements in order to account for air in the firn lowering the conductivity. These corrections was able to bring out the increased conductivity due to industrial activities in the mid 20^{th} century otherwise hidden, but at the same time took away the possibility to constrain the NEGIS major ion balance, as the correct relation between acidity and ECM/DEP response was not known. The different conductivity measures agreed reasonably well in acidic ice, but a few times large ammonium spikes occurred, that caused the solution to be alkaline. Here the ECM value decreased to an equivalent of 0 μM H^+, while electrolytic conductivity, liquid as well as DEP, was increased.

7.1 Future work

Being the first continuous record of DRP and direct pH measures, only a very few sources were available for comparison and validation of results. To improve on the strength of the findings, data series from other drill sites should be included for comparison, even though no similar measurements are available. As an example, a comparison between records of

vanillic acid in ice cores and a list of major forest fires, might be used to validate whether the years where spikes was found in the NEGIS core coincides with forest fire signals in the Greenland ice cores. Likewise, if details of the relation between firn density and ECM/DEP response were better understood, it might be possible to reinterpret the NEGIS findings and constrain the major ion balance at the site.

Bibliography

Alley, R. B. and Anandakrishnan, S. (1995). Variations in melt-layer frequency in the GISP2 ice core: implications for Holocene summer temperatures in central Greenland. *Annals of Glaciology*, 21:64–70.

Atkins, P. and Jones, L. (2010). *Chemical Principles – The Quest fot Insight*. Clancy Marshall, 5. international edition.

Barnes, P. R. F., Wolff, E. W., Mulvaney, R., Udisti, R., Castellano, E., Röthlisberger, R., and Steffensen, J.-P. (2002). Effect of density on electrical conductivity of chemically laden polar ice. *Journal of Geophysical Research: Solid Earth*, 107(B2):ESE 1–1–ESE 1–14.

Bigler, M., Svensson, A., Kettner, E., Vallelonga, P., Nielsen, M. E., and Steffensen, J. P. (2011). Optimization of high-resolution continuous flow analysis for transient climate signals in ice cores. *Environmental Science & Technology*, 45(10):4483–4489.

Bolin, B., Crutzen, P., Vitousek, P., Woodmansee, R., Goldber, E., and Cook, R. (1981). SCOPE 21, The Major Biogeochemical Cycles and their Interactions – chapter 1: Interactions of Biogeochemical Cycles. *Workshop on the Interactions of Biogeochemical Cycles*.

Centre for Ice and Climate (2013a). http://www.iceandclimate.nbi.ku.dk/research/flowofice/.

Centre for Ice and Climate (2013b). http://www.iceandclimate.nbi.ku.dk/research/drill_analysing/cutting_and_analysing_ice_cores/.

ChemBuddy (2013). http://www.chembuddy.com/?left=pH-calculation&right=water-ion-product.

Cole-Dai, J. (2010). Volcanoes and climate. *Wiley Interdisciplinary Reviews: Climate Change*, 1(6):824–839.

Edwards, R., McConnell, J. R., and Banta, J. R. (2007). Atmospheric Deposition of Iron and Phosphorus to Greenland over the 20th- Century. *AGU Fall Meeting Abstracts*, page B1154.

Estela, J. M. and Cerdá, V. (2005). Flow analysis techniques for phosphorus: an overview. *Talanta*, 66:307–331.

Filippelli, G. M. (2002). The global phosphorus cycle. *Reviews in Mineralogy and Geochemistry*, 48(1):391–425.

Filippelli, G. M. (2008). The Global Phosphorus Cycle: Past, Present, and Future. *Elements*, 4(2):89–95.

Fuhrer, K., Neftel, A., Anklin, M., Staffelbach, T., and Legrand, M. (1996). High-resolution ammonium ice core record covering a complete glacial inter-glacial cycle. *J. Geophys. Res.*, 101:4147–4164.

Hammer, C. (1980). Acidity of polar ice cores in relation to absolute dating, past volcanism, and radio-echoes. *Journal of Glaciology*, 25(93):359–372.

Hodson, A., Mumford, P., and Lister, D. (2004). Suspended sediment and phosphorus in proglacial rivers: bioavailability and potential impacts upon the P status of ice-marginal receiving waters. *Hydrological Processes*, 18(13):2409–2422.

Karlöf, L., Winther, J.-G., Isaksson, E., Kohler, J., Pinglot, J. F., Wilhelms, F., Hansson, M., Holmlund, P., Nyman, M., Pettersson, R., Stenberg, M., Thomassen, M. P. A., van der Veen, C., and van de Wal, R. S. W. (2000). A 1500 year record of accumulation at Amundsenisen western Dronning Maud Land, Antarctica, derived from electrical and radioactive measurements on a 120 m ice core. *Journal of Geophysical Research: Atmospheres*, 105(D10):12471–12483.

Kaufmann, P. R., Federer, U., Hutterli, M. A., Bigler, M., Sch¨upbach, S., Ruth, U., Schmitt, J., and Stocker, T. F. (2008). An improved continuous flow analysis system for high-resolution field measurements on ice cores. *Environmental Science & Technology*, 42(21):8044–8050.

Kjær, H. A., Svensson, A., Vallelonga, P., Kettner, E., Schüpbach, S., Bigler, M., Steffensen, J. P., and Hansson, M. E. (2011). First continuous phosphate record from Greenland ice cores. *Climate of the Past Discussions*, 7(6):3959–3989.

Kjær, H. A. (2010). Phosphate in Ice Cores – Finding a method for continuous detection of phosphate in ice cores. Master's thesis, Centre for ice and Climate, University of Copenhagen.

Kjær, H. A. (2013). Personal communication.

Kjær, H. A., Vallelonga, P., Svensson, A., Kristensen, M., Tibuleac, C., and Bigler, M. (2012a). A continuous flow analysis method for determination of dissolved reactive phosphorus in ice cores. Sent to: Environmental Science & Technology.

Kjær, H. A., Vallelonga, P. T., Meusinger, C., Johnson, M. S., and Svensson, A. (2012b). Continuous detection method (CFA) for pH in ice cores. In *IPICS – International Partnership in Ice Core Sciences: first open science conference*.

Kuramoto, T., Goto-Azuma, K., Hirabayashi, M., Miyake, T., Motoyama, H., Dahl-Jensen, D., and Steffensen, J. P. (2011). Seasonal variations of snow chemistry at NEEM, Greenland. *Annals of Glaciology*, 52:193–200.

Larsen, L. B., Simon, S. G., and Steffensen, J. (2012). Field season 2012: North Greenland Eemian Ice drilling – NEEM 4th and last season of deep ice core drilling. Technical report, Center for Ice and Climate, University of Copenhagen.

Mahowald, N., Jickells, T. D., Baker, A. R., Artaxo, P., Benitez-Nelson, C. R., Bergametti, G., Bond, T. C., Chen, Y., Cohen, D. D., Herut, B., Kubilay, N., Losno, R., Luo, C., Maenhaut, W., McGee, K. A., Okin, G. S., Siefert, R. L., and Tsukuda, S. (2008). Global distribution of atmospheric phosphorus sources, concentrations and deposition rates, and anthropogenic impacts. *Global Biogeochemical Cycles*, 22(4).

Mahowald, N. M., Baker, A. R., Bergametti, G., Brooks, N., Duce, R. A., Jickells, T. D., Kubilay, N., Prospero, J. M., and Tegen, I. (2005). Atmospheric global dust cycle and iron inputs to the ocean. *Global Biogeochemical Cycles*, 19(4):n/a–n/a.

McConnell, J. R., Edwards, R., Kok, G. L., Flanner, M. G., Zender, C. S., Saltzman, E. S., Banta, J. R., Pasteris, D. R., Carter, M. M., and Kahl, J. D. W. (2007). 20th-Century Industrial Black carbon emissions altered arctic climate forcing. *Science*, 317:1381.

Millero, F. J., Graham, T. B., Huand, F., Bustos-Serrano, H., and Pierrot, D. (2006). Dissociation constants of carbonic acid in seawater as a function of salinity and temperature. *Marine Chemistry*, 100(4):80–94.

Moore, J. C., Mulvaney, R., and Paren, J. G. (1989). Dielectric stratigraphy of ice: A new technique for determining total ionic concentrations in polar ice cores. *Geophysical Research Letters*, 16(10):1177–1180.

Moore, J. C., Wolff, E. W., Clausen, H. B., and Hammer, C. U. (1992). The Chemical Basis for the Electrical Stratigraphy of Ice. *J. Geophys. Res.*, 97(B2):1887–1896.

Moore, J. C., Wolff, E. W., Clausen, H. B., Hammer, C. U., Legrand, M. R., and Fuhrer, K. (1994). Electrical response of the Summit-Greenland ice core to ammonium, sulphuric acid, and hydrochloric acid. *Geophysical Research Letters*, 21(7):565–568.

National Institute of Standards and Technology (2013). http://webbook.nist.gov/cgi/cbook.cgi?ID=C124389&Mask=10#Solubility.

Nenes, A., Krom, M., Mihalopoulos, N., Van Cappellen, P., Shi, Z., Bougiatioti, A., Zarmpas, P., and Herut, B. (2011). Atmospheric acidification of mineral aerosols: a source of

bioavailable phosphorus for the oceans. *Atmospheric Chemistry and Physics Discussions*, 11(2):6163–6185.

Pasteris, D. R., McConnell, J. R., and Edwards, R. (2012). High-Resolution, Continuous Method for Measurement of Acidity in Ice Cores. *Environmental Science & Technology*, 46(3):1659–1666.

Pasteris, D. R., McConnell, J. R., Edwards, R., and Banta, R. (2009). A Novel Technique for High Resolution Ice Core Acidity Measurements. Poster from Desert Research Institute, Rene, Nevada.

Paterson, W. and Cuffey, K. (2010). *The Physics of Glaciers*. Academic Press, 4. edition.

Paytan, A. and McLaughlin, K. (2007). The Oceanic Phosphorus Cycle. *Chem. Rev.*, 107:563–576.

Raghuraman, B., Gustavson, G., Van Hal, R. E. G., Dressaire, E., and Zhdaneev, O. (2006). Extended-Range Spectroscopic pH Measurement Using Optimized Mixtures of Dyes. *Appl. Spectrosc.*, 60(12):1461–1468.

Rasmussen, S. O., Andersen, K. K., Johnsen, S. J., Bigler, M., and McCormack, T. (2005). Deconvolution-based resolution enhancement of chemical ice core records obtained by Continuous Flow Analysis. *Journal of Geophysical Research: Atmospheres*, 110(D17).

Smil, V. (2002). *Phosphorus: Global Transfers*, volume 3. John Wiley & Sons.

Sugiyama, K., Fujita, S., Narita, H., Mae, S., Hondoh, T., Goto-Azuma, K., Fisher, D. A., and Koerner, R. M. (2000). Measurement of electrical conductance in ice cores by ac-ecm method. In *Measurement of electrical conductance in ice cores by AC-ECM method*, pages 173 – 184. Hokkaido University Press.

Taylor, K., Alley, R., Fiacco, J., Grootes, P., Lamorey, G., Mayewski, P., and Spencer, M. J. (1992). Ice-core dating and chemistry by direct-current electrical conductivity. *Journal of Glaciology*, 38:325–332.

Turekian, K. K. (1968). *Oceans*. Prentice-Hall.

van den Broeke, M., Bamber, J., Ettema, J., Rignot, E., Schrama, E., van de Berg, W., van Meijgaard, E., Velicogna, I., and Wouters, B. (2009). Partitioning Recent Greenland Mass Loss. *Science*, 326(5955):984–986. Publisher: AAAS.

Wikipedia (2013a). http://en.wikipedia.org/wiki/List_of_wildfires.

Wikipedia (2013b). http://en.wikipedia.org/wiki/List_of_fires.

Wolff, E. (2000). Electrical stratigraphy of polar ice cores: principles, methods, and findings. In Hondoh, T., editor, *Physics of ice core records*, pages 155–171. Hokkaido University Press, Sapporo.

List of Figures

List of Tables

Acidity equations

The following is the acidity equations used to calculate the concentration of hydrogen ions contributed by CO_2 in the pH signal. The equations can be found in [Pasteris et al., 2012, supporting information] and [Atkins and Jones, 2010]. K_w is the water autoprotolysis constant and K_H is the Henry's dissociation constant.

$$\text{acidity} = \left[H^+\right] - \left[HCO_3^-\right] - 2\left[CO_3^{2-}\right] - \left[OH^-\right] \tag{1}$$

which can be rewritten as

$$\text{acidity} = \left[H^+\right] - \frac{K_H P_{CO_2}}{\alpha_0}(\alpha_1 + 2\alpha_2) - \frac{K_w}{\left[H^+\right]} \tag{2}$$

$$C_T = \text{total cabonate} = \frac{K_H P_{CO_2}}{\alpha_0} \tag{3}$$

$$\alpha_0 = H_2CO_3 \text{ ionization fraction} = \left(1 + \frac{K_1}{\left[H^+\right]} + \frac{K_1 K_2}{\left[H^+\right]^2}\right)^{-1} \tag{4}$$

$$\alpha_1 = HCO_3^- \text{ ionization fraction} = \left(1 + \frac{\left[H^+\right]}{K_1} + \frac{K_2}{\left[H^+\right]}\right)^{-1} \tag{5}$$

$$\alpha_2 = CO_3^{2-} \text{ ionization fraction} = \left(1 + \frac{\left[H^+\right]}{K_2} + \frac{\left[H^+\right]^2}{K_1 K_2}\right)^{-1} \tag{6}$$

The Henry's law constant is a function of the temperature, and can be calculated using the formula, [National Institute of Standards and Technology, 2013]:

$$K_{\mathrm{H}}(T) = 0.034 \cdot \exp\left(2400\ \mathrm{K} \cdot \left(\frac{1}{T} - \frac{1}{298.15\ \mathrm{K}}\right)\right), \tag{7}$$

where T is the temperature on the Kelvin scale. Likewise the dissociation constants vary with the temperature and the salinity. However, the salinity in ice cores is usually very low, and may be assumed to be zero. Empirical formulas for the dissociation constants has been found by e.g. [Millero et al., 2006], in the form

$$\mathrm{p}K_1 = -126.34048 + 6320.813/T + 19.568224 \cdot \ln(T) \tag{8}$$

$$\mathrm{p}K_2 = -90.18333 + 5143.692/T + 14.613358 \cdot \ln(T) \tag{9}$$

The autoprotolysis constant, K_{w}, is also highly temperature dependant, and the values for this constant can be found tabulated e.g. using [ChemBuddy, 2013]. However, the overall magnitude of this constant is very small as compared to the other components of equation (2), and hence the variability is not very important. A plot of the CO_2 contributed hydrogen ions as a function of temperature, with variations in the partial CO_2 pressure can be seen in figure 25 below.

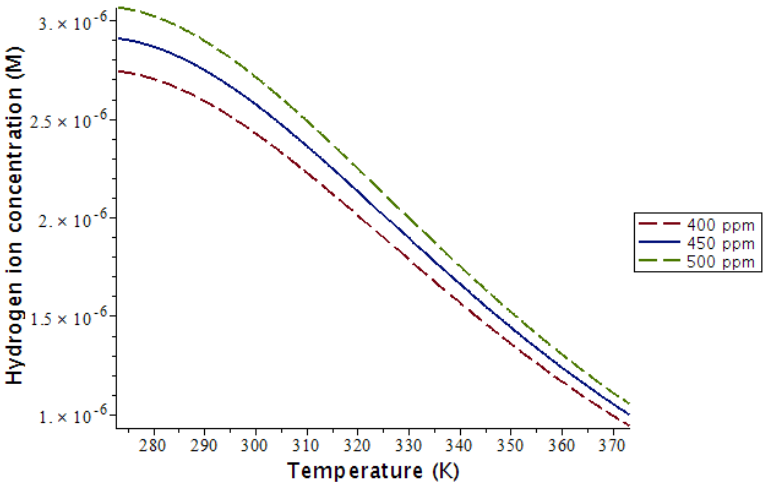

Figure 25: Calibration curve for CO_2. On the axis is the temperature and the hydrogen ion concentration contributed by the partial CO_2 pressure. The different curves correspond to different partial pressures of CO_2.

Response times

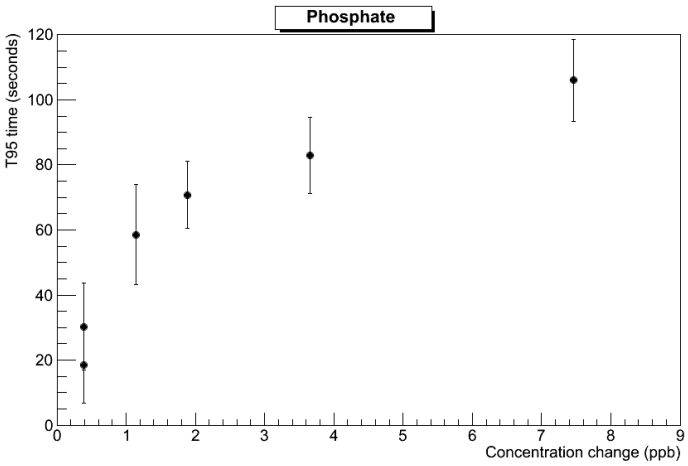

Figure 26: Response times for phosphate measurements, as magnitude of change in concentration vs. the 5 % to 95 % reaction time.

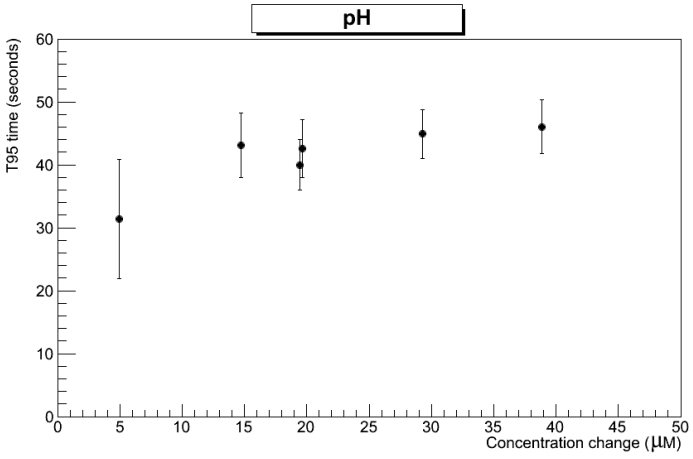

Figure 27: Response times for pH measurements, as magnitude of change in concentration vs. the 5 % to 95 % reaction time.

Running correlations

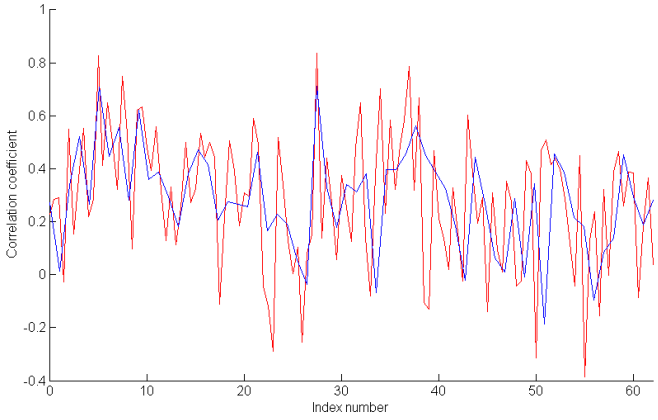

Figure 28: Running correlation of PO_4^{3-} vs. dust. On the axis is the index number, which is essentially the length of the core processed. The red curve uses intervals of 0.5 meters to calculate corelations, while the blue curve uses intervals of 1 meter. On the abscisse axis is the correlation coefficient in that interval.

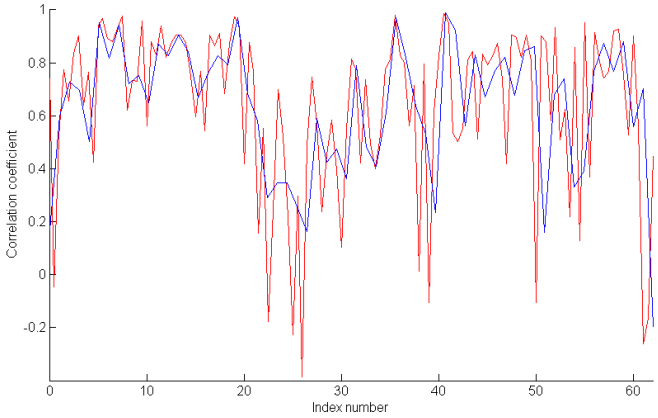

Figure 29: Running correlation of pH vs. liquid conductivity. The axes are the same as for figure 28 above.